Hyperelastic nature of Hoek-Brown criterion

Ilaria Fontana, Kyrylo Kazymyrenko, Daniele Di Pietro

Hyperelastic nature of the Hoek–Brown criterion

Ilaria Fontana*[,1], Kyrylo Kazymyrenko[2], and Daniele A. Di Pietro[3]

[1]Department of Engineering Sciences and Applied Mathematics, Northwestern University, Evanston, IL 60208, USA
[2]UMR EDF-CNRS-CEA-ENSTA 9219, IMSIA, Palaiseau, France
[3]IMAG, Univ Montpellier, CNRS, Montpellier, France

Abstract

We analyze the transition from the nonlinear elastic behavior to the elasto-plastic one. A specific class of what we call hyperbolic elasticity arises from theoretical considerations as a straight consequence of the yield criterion invariance on plasticity level. The latter property of fixed yield residual plasticity is observed experimentally for many geomaterials. We superimpose this nonlinear elastic (or hyperelastic) hypothesis on the plastic constitutive relation. Curiously, we found that the hyperbolic nonlinearity, introduced through the Standard Generalized Material formalism, affects the residual yield surface shape. In particular, the initially linear surface curves to a quadratic one, establishing correspondence between Mohr–Coulomb and Hoek–Brown (or alternatively between Drucker–Prager and Pan–Hudson) criteria. Our first conclusion is that one possible justification of the empirical fitted Hoek–Brown criterion widely used in geoscience is the material's hyperelastic nature. We compare further elasto-plastic responses of standard tests for Drucker–Prager constitutive relation with both linear and nonlinear elastic phases. Most notably, the nonlinear case distinguishes itself by the dilatancy saturation and accommodation phenomena during cyclic loading in the triaxial compression test. This rather complex experimentally observed behavior emerges straight from the nonlinear unloading property in the elasto-plastic description.

Keywords: hyperelasticity, elasto-plastic model, hyperbolic elasticity, Hoek–Brown and Drucker–Prager criteria, Pan–Hudson criteria, small rotations

MSC2020 classification: 74B20, 74C05

1 Introduction

One of the key points in the accurate description of rocks is the precise identification of their elastic domain (or yield surface/criterion). Due to the softening behavior, not only rocks but also all analogous materials like concrete, clay, soil or even ice [43] are commonly classified by their resistance to various mixed-mode loading. This approach is closely related to the basic safety rules in industrial applications, where it is often considered that geomaterials could exhibit unstable failure once the critical loading is reached [17].

Throughout the last century, specific testing machines and corresponding measurement protocols were established by national and international committees in order to harmonize

*Corresponding author: ilaria.fontana@northwestern.edu

and standardize the experimental characterization of the above-cited brittle materials. To mention only a few, the Brazilian tensile [3], oedometric, uni- and tri-axial compression are all well-documented experiments that are routinely executed to catalog material strength by spotting just some points of their multidimensional yield surface. This reduced "single point" vision of material resistance is increasingly scrutinized in recent times, and multiple evolutions have been adopted. For instance, constant improvements of finite element software enable new kinds of modeling, with loadings going beyond the elastic domain to explore a more subtle post-peak behavior. In the corresponding mechanical tests, the response of the material subjected to a set of pre-established loadings is analyzed during both the elastic and softening phase, enabling the full model parameter fitting. Some more sophisticated hybrid measurement techniques are also proposed, where the loading path is adapted during the test execution. A single, all-in-one experiment replaces the classical set with the same goal of full model identification [22]. While the complexity of post-peak description could be reached through various theoretical formalisms, most of them still rely on the initial yield surface definition, and the question of this elastic domain shape remains the cornerstone of any nonlinear model identification. Even if considerable progress was made in recent decades, this precise identification of the yield surface remains nowadays a rather challenging task [26].

A common feature of geomaterials is their strong resistance to compressive loading. For some large-scale structures, like hydraulic dams or underground tunnel excavations, the construction material is naturally submitted to high levels of compression. For others, like nuclear confinement buildings or bridges, civil engineering constitutive concrete parts are preloaded to reach artificially an initial compression state by supplementary constraint of tension reinforcing steel tendons. In both cases, the property of higher compressive resistance is exploited on the industrial level with the aim of increasing global structure robustness.

According to the physical origin of geomaterials, a large variety of criteria defining the elastic domain are employed in order to model their mechanical behavior. The simplest surface, admitting infinite resistance in hydrostatic compression, is the linear cone-shaped one. It was first introduced more than a century ago [31] as the combination of Coulomb's friction hypothesis [5] with Galileo–Rankine's tension cut-off principle. The initial principal stress description, which is commonly called the Mohr–Coulomb shape, was later generalized in the work of Drucker and Prager to a more smooth deviator-trace relation [7]. The straight relation between shear and compressive loadings, which is the main signature of these linear criteria, has allowed the development of various constitutive relations based on the same simplified dependence [1, 24].

In the middle of the last century, with numerous large infrastructural projects ongoing, more complex criteria emerged as further experimental data became available. For wider ranges of loadings, the friction-type shear dependency seemed to be deflecting from the linear curve. Logically, a quadratic relation was to be explored first. Back in 1924, assuming the hypothesis of crack propagation via rapid growth of randomly distributed micro-flaws, Griffith had already obtained a theoretical justification of the parabolic yield shape [13]. Inspired by Griffith's model, Fairhurst proposed its empirical extension validated on the tensile Brazilian test [10]. In this spirit, in 1980 Evert Hoek and Edwin T. Brown [16] came up with a new particular shape of quadratic nonlinear criterion. It reproduced the Mohr–Coulomb-type singularity for weak tensile loading simultaneously taking into account the reduction of shear resistance for high compression. Purely empirical, the Hoek–Brown criterion was originally obtained for intact rocks by two parameters fitting

the results of triaxial tests. Validated during the following years on a wider experimental database, the criterion was used extensively in the design of underground excavations [17].

It should be underlined that not only previously cited [13, 10, 16], but many other authors (e.g. Pan–Hudson [34]) kept the number of model parameters reduced so that a better fit was obtained by the new curve's form itself, rather than by the addition of supplementary fitting variables. Consequently, the final expression of the failure criteria, being the pure result of the trial-error process, appears quite artificial at first glance. *In this article, we try to establish a possible hyperelastic link between the whole class of quadratic Hoek–Brown (Pan–Hudson) type criteria and their linear Mohr–Coulomb (Drucker–Prager) counterparts.* The single hypothesis of the existence of a stable failure surface under free-energy based description generates a subclass of quadratic yield surfaces from the linear relation of the generalized plastic force. The Hoek–Brown relation is seen then as a consequence of the simultaneous presence of both plasticity and nonlinear elasticity phenomena in the geomaterial under investigation. We argue, finally, that the cyclic triaxial compression test plays a particular role in the material classification as it reveals the eventual presence of nonlinear elasticity.

2 Hyperelasticity coupled to plasticity

In this section, we summarize the main idea of the article, reducing as far as possible technical details and complex notation that are required for a rigorous theoretical description of so-called "simple materials" [40, Chapter IV]. Our main aim is to establish an isothermal homogeneous isotropic constitutive relation for rock-like materials satisfying some basic thermodynamic principles. A more detailed description of the formalism and notations can be found in [38, Chapter 2], [39, Chapter 7], or [20].

Plasticity is known to be one of the main sources of nonlinearity. For high compression levels, nonlinearity is observed for elastic unloading as well. In geoscience applications, both processes influence the resulting material nonlinearity. From the modeling side, the most common approaches are treating both sources of nonlinearity in a separate way: either the plasticity is introduced in *infinitesimal* strain models admitting trivial linear unloading, or alternatively the nonlinearity is seen to be of pure hyperelastic origin and is taken into account with help of *finite* strain description. While hyperelasticity was extensively studied for large strains in the past, its extension to coupled elasto-plasticity is anything but trivial (see some classical books [40, 33]). In the current paper, we propose a simple formalism particularly adapted for geomaterials establishing a link between these two physical phenomena. We will focus mainly on the yield surface modification generated by the presence of nonlinear elasticity. In particular, we found that the supplementary hypothesis of non-evolving with plasticity reversible stress domain leads to some specific hyperelastic behavior and shows how it can be revealed experimentally.

In what follows we discuss first the phenomenological justification of chosen theoretical description, for readers familiar with the topic we advise to skip straight to section 2.3.

2.1 Internal variable choice

If classical mechanics aims to associate the body kinematic to the applied forces, in its quasi-static extension for the continuum media the body deformation represented by the displacement field is connected to the density of forces. Two physical quantities naturally arise: the first is the Cauchy stress tensor $\boldsymbol{\sigma}$, which characterizes the state of internal

forces; the second is the strain tensor $\boldsymbol{\varepsilon}$, which measures the level of deformation up to some reference configuration [21] (also called placement [40]). For instance, in the absence of residual stresses, it is implicitly assumed that the reference configuration can be obtained by complete mechanical unloading, mapping the initial state to a zero strain. The existence of this "placement at ease" in general is not guaranteed [40, Chapter IV.5], but if it is known, both of the quantities (i.e. strain and stress) are objective and experimentally measurable. Consequently, one of the goals of continuum mechanics is to establish a link between these two second-order tensors, which is named material constitutive relation (see [40, 21, 38]).

The Cauchy elasticity, in the most simple way, postulates that the stress is some function of the strain: $\boldsymbol{\sigma} = \boldsymbol{\sigma}(\boldsymbol{\varepsilon})$, [40]. For isotropic materials the most general relation is derived by applying Rivlin–Ericksen representation theorem, which gives for three-dimensional space:

$$\boldsymbol{\sigma} = c_0\mathbf{I}_2 + c_1\boldsymbol{\varepsilon} + c_2\boldsymbol{\varepsilon}^2, \tag{2.1}$$

where $\mathbf{I}_2$ is the identity tensor and c_i are some scalar functions of the eigenvalues of the strain tensor $\boldsymbol{\varepsilon}$, or equivalently of its rotational invariants. Up until now, we had no need to specify which particular expression for strain is to be taken (Green–Lagrange, Euler–Almansi, infinitesimal strain, etc.), but once the small deformation hypothesis is applied the strain expression is linearized, so that it becomes equal to the symmetric part of the gradient of the displacement field. Under this assumption all the higher order terms are neglected resulting in well known Hooke's stress-strain relation: $\boldsymbol{\sigma} = \lambda \mathrm{Tr}\,\boldsymbol{\varepsilon}\,\mathbf{I}_2 + 2\mu\boldsymbol{\varepsilon} \equiv \mathbb{E}\boldsymbol{\varepsilon}$, where λ, μ are the two constant Lamé parameters, that characterize linear elasticity.

For geomaterials, even within the elastic phase, we need to go beyond this trivial linear constitutive relation by introducing some nonlinearity in the stress-strain relation [21]. A very common approach consists of the analysis of initial quadratic Rivlin–Ericksen expression making use of finite strain (Green–Lagrange, Euler–Almansi, etc.) or finite deformation tensors (Cauchy–Green, Finger, etc.). A description relying exclusively on infinitesimal strain $\boldsymbol{\varepsilon}$ becomes physically questionable, as it generates non-zero stresses for pure rigid body rotation (consider, for example, unstretched central inversion transformation with infinitesimal strain $\boldsymbol{\varepsilon} \sim \mathbf{I}_2 \neq \mathbf{0}$). The second-order contributions ($\sim \boldsymbol{\varepsilon}^2$) reappear in the perturbation theory, but the exclusive infinitesimal strain dependence ($\boldsymbol{\sigma} = \boldsymbol{\sigma}(\boldsymbol{\varepsilon})$) imposes important constraints on the elastic constitutive relation as a whole [40, Chapter IX.6].

Regardless of all these limitations, the infinitesimal strain $\boldsymbol{\varepsilon}$ is still of widespread use in experimental geoscience, even for its values going up to $20\% - 30\%$. One of the reasons for this is that, in most tests or studies, specific boundaries are applied reducing rotation influence. In the case of infinitesimal rotations, one can still rely on the symmetric gradient of displacement as an objective deformation measure even for finite stretching: while the tensors of Green–Lagrange and symmetric gradient stresses are equal up to the first order of infinitesimal rotations, all of their rotational invariant (hydrostatic parts $\mathrm{Tr}\,\boldsymbol{\varepsilon}$, deviator, determinant) are equivalent even up to the second order, see the Appendix B. Provided that the rotations are small, the elastic nonlinearity of the constitutive relation can be incorporated into the model description through an infinitesimal strain dependence and this is without alternating its objectivity. This approach was already used in the past theoretical works for soils and clays [21, 32] and it will be adopted throughout the current paper as well. It sounds coherent for geoscience applications in general as, first, we do not expect the underground tunnel or hydraulic dam to rotate significantly before failure and, second, the material's nonlinearity is more easily revealed by a high level of hydrostatic

compression common to this industry.

In order to shorten our notations, up from now $\boldsymbol{\varepsilon}$ *will be referred to as the symmetric part of the gradient of displacement field* $\boldsymbol{u}$*, i.e., we consider the classical infinitesimal strain expression*: $\boldsymbol{\varepsilon} = (\nabla \boldsymbol{u} + (\nabla \boldsymbol{u})^{\dagger})/2$.

In principle, the general Rivlin–Ericksen stress-strain relation presented earlier is recovered. But it should be noted, that not any kind of stress-strain relation is admissible from a thermodynamical point of view. For instance, the work of internal forces for constitutive relations with non-symmetric tangent operator $\partial\boldsymbol{\sigma}/\partial\boldsymbol{\varepsilon}$ is dependent on the loading path, which is physically inadmissible for a fully reversible elastic process (consider for example $\boldsymbol{\sigma} \sim \mathrm{Tr}\,(\boldsymbol{\varepsilon})\,\boldsymbol{\varepsilon}$). The hyperelasticity restricts this stress-strain relationship by admitting the existence of a scalar strain energy density function ϕ from which the stress is derived: $\boldsymbol{\sigma} = \partial\phi/\partial\boldsymbol{\varepsilon}$, [38, 39]. Mechanical loading of a hyperelastic material is considered as a zero dissipation reversible process with the sole state variable being strain $\boldsymbol{\varepsilon}$. In this sense, the hyperelastic formalism is conservative and is compatible with a general thermodynamical description [12]. If the equivalence between strain and stress description is not necessarily satisfied for finite transformations (see [40, Chapter VII.3]), it is usually admitted for small ones. For smooth convex strain energy density function, the bijective nature of the stress-strain relation is automatically satisfied and realized via Legendre transformation.

In order to take properly into account the energy dissipation process, which is definitely present for geomaterials, at least one supplementary state variable needs to be introduced. It is usually done through the plastic strain tensor $\boldsymbol{p}$, which is supposed to decompose the strain into elastic and plastic contributions, i.e., $\boldsymbol{\varepsilon} = \boldsymbol{\varepsilon}^{\mathrm{el}} + \boldsymbol{p}$ (for sake of clarity, from now on $\boldsymbol{\varepsilon}$ will be called *total strain*). This notion of strain shift appears naturally for infinitesimal deformations, as the reference configuration change engenders an additive translation of actual strain value: $\boldsymbol{\varepsilon} \Rightarrow \boldsymbol{\varepsilon} + \boldsymbol{\varepsilon}_{ref}$, where $\boldsymbol{\varepsilon}_{ref}$ is the strain compatible with the "old to new" reference configuration displacement. Therefore, even for a purely elastic model, a supplementary state variable $\boldsymbol{\varepsilon}_{ref}$ can be introduced with the aim of describing a "placement at ease". If the latter is unachievable through simple elastic unloading (i.e., is incompatible with a continuous displacement field), the plastic strain $\boldsymbol{p}$ can be seen as a history variable tracing the anelastic reference configuration transformation: $\boldsymbol{\varepsilon}_{ref} \Rightarrow \boldsymbol{p}$. The sole hypothesis made at this level is that tensor $\boldsymbol{p}$ is eventually incompatible with any kind of displacement field. Then, the plastic strain has a clear physical meaning of an incompatible part of the residual strain that cannot be suppressed by a suitable reference configuration choice or a total system unloading. The plastic strain $\boldsymbol{p}$ is generally not directly observable, which is why it is also called an internal (hidden or memory) state variable. Some authors suppose further that the Cauchy stress depends only on the elastic strain, which allows its indirect measurement: $\boldsymbol{\sigma} \Rightarrow \boldsymbol{\varepsilon}^{\mathrm{el}} = \boldsymbol{\varepsilon} - \boldsymbol{p}$. In this sense, the elastic strain $\boldsymbol{\varepsilon}^{\mathrm{el}}$ becomes an observable (in general a hidden one), and the couple of state variables $(\boldsymbol{\varepsilon}, \boldsymbol{p})$ can be replaced by the following pair $(\boldsymbol{\varepsilon}_{\mathrm{el}}, \boldsymbol{p})$. The stress invariance to reference configuration choice implies necessarily an induced shift of plastic strain by $\boldsymbol{\varepsilon}_{\mathrm{ref}}$: $\boldsymbol{\varepsilon} \to \boldsymbol{\varepsilon} + \boldsymbol{\varepsilon}_{\mathrm{ref}} \Rightarrow \boldsymbol{p} \to \boldsymbol{p} + \boldsymbol{\varepsilon}_{\mathrm{ref}}$. For the situation where the observation of the material starts at the point with a non-negligible initial plastification level, any constitutive relation becomes ill-defined in the sense of simple media [40]. Indeed, the plastic strain does depend on $\boldsymbol{\varepsilon}_{\mathrm{ref}}$, violating then the history-independence hypothesis, unless the at-ease configuration can be somehow back-traced from the current state. In particular, for commonly used elasto-plastic models with linear elastic phase, the initial state is unrecoverable. There is no way to distinguish a boundary compatible transformation of the at-ease configuration $\boldsymbol{\varepsilon}_{\mathrm{ref}}^{\mathrm{comp}}$ from equivalent modification of the plastic strain: $\boldsymbol{\varepsilon} - \boldsymbol{p} \equiv (\boldsymbol{\varepsilon} + \boldsymbol{\varepsilon}_{\mathrm{ref}}^{\mathrm{comp}}) - (\boldsymbol{p} + \boldsymbol{\varepsilon}_{\mathrm{ref}}^{\mathrm{comp}})$. The

ambiguity of total and plastic strain definition up to an unmeasurable arbitrary shift in the reference state can be lifted for a bijective constitutive relation (see full discussion in [37]). For pure plasticity (i.e. plasticity being a single internal variable), the choice of elastic strain instead of total strain as state variable can be assimilated with the simple strain to stress variable change, as both are related via unchanged elastic moduli: $(\boldsymbol{\varepsilon}_{\mathrm{el}}, \boldsymbol{p}) \Rightarrow (\boldsymbol{\sigma}, \boldsymbol{p})$. This leads to the well-known Gibbs-like description in thermodynamics. Nevertheless, the presence of elastic nonlinearity or of any kind of additional irreversible dissipative phenomena makes the internal variable choice less trivial and highly impactful, especially when thermodynamic considerations are taken into account.

As we will show later in this paper, for geomaterials that exhibit a nonlinear reversible elastic phase (i.e., the presence of hyperelasticity), the choice of total and plastic strains as state variables seems to be particularly adapted. Not only it allows labeling the reference configuration due to nonlinearity at any given plasticity level, but also opens the way for various model extensions either by enriching its complexity through a new internal variable introduction, such as damage-plasticity coupling [25, 30], or by regularizing its deformation in the critical state [11].

2.2 Simplified thermodynamics

The thermodynamical description of continuum mechanics relies either on the Helmholtz free energy density definition [12] or alternatively on Gibbs free energy [4, 20]. The existence of such energy function state may be derived from the more basic Work Principle introduced in [29] that appears naturally for any continuum mechanical system. For isothermal evolution in the presence of plasticity, this function depends on at least two state variables. We make the choice of Helmholtz description with the total strain $\boldsymbol{\varepsilon}$ and the plastic strain $\boldsymbol{p}$ as state variables, i.e., $\phi(\boldsymbol{\varepsilon}, \boldsymbol{p})$ represents the free energy. The Cauchy stress tensor is then the dual conjugate to the total strain $\boldsymbol{\sigma} = \partial\phi/\partial\boldsymbol{\varepsilon}$, while the energy response of the system to plastic strain evolution is captured through the generalized plastic force $\boldsymbol{X} = -\partial\phi/\partial\boldsymbol{p}$. As it was mentioned above, most of the elasto-plastic models admit additive separation of elastic and plastic strains, resulting in the simplest quadratic expression for the free energy of the residual plastic state:

$$\phi(\boldsymbol{\varepsilon}, \boldsymbol{p}) = \frac{1}{2}\mathbb{E}(\boldsymbol{\varepsilon} - \boldsymbol{p})^2, \tag{2.2}$$

where $\mathbb{E}$ is the constant elastic modulus which depends on the Lamé parameters λ and μ. Notice that for simplicity we adopt the abridged notations for tensor operations. In particular, in this linear elastic case, the generalized plastic force and Cauchy stress are equal:

$$\boldsymbol{\sigma} = \boldsymbol{X} = \mathbb{E}(\boldsymbol{\varepsilon} - \boldsymbol{p}). \tag{2.3}$$

The reversible elastic domain, characterized by the absence of plasticity evolution, is defined in the observable stress space: $\boldsymbol{p} = \mathrm{const} \Rightarrow \boldsymbol{\sigma} \in \mathbb{K}_{\boldsymbol{\sigma}}$. In addition, thermodynamically, one needs to ensure that the material dissipation rate, or alternatively called interior work [29], is positive:

$$\mathcal{D} = \boldsymbol{\sigma}\dot{\boldsymbol{\varepsilon}} - \dot{\phi}(\boldsymbol{\varepsilon}, \boldsymbol{p}) \geq 0, \tag{2.4}$$

where the dot corresponds to the temporal derivative, i.e., $\dot{\boldsymbol{\varepsilon}} \equiv d\boldsymbol{\varepsilon}/dt$. Considering elastic unloading first, we obtain the $\boldsymbol{\sigma} = \partial\phi/\partial\boldsymbol{\varepsilon}$ relation as consequence of zero dissipation

process $\mathcal{D}(\boldsymbol{p} = \text{const}) = 0$, reducing then the second thermodynamic principle (2.4) to the following straight inequality:

$$\mathcal{D} = -\frac{\partial \phi}{\partial \boldsymbol{p}} \dot{\boldsymbol{p}} = \boldsymbol{X} \dot{\boldsymbol{p}} \geq 0. \tag{2.5}$$

As we have mentioned in the introduction, considerable experimental efforts are focused on the identification of the elastic domain. In the perfect plasticity hypothesis, the domain is fixed during evolution and its shape can consequently be considered one of the main material properties. It is clear that, for the linear case described above (i.e., $\mathbb{E}$ constant), the stress domain is identical to the generalized force domain: $\boldsymbol{p} = \text{const} \Rightarrow \boldsymbol{\sigma} \in \mathbb{K}_{\boldsymbol{\sigma}}$ or equivalently $\boldsymbol{X} \in \mathbb{K}_{\boldsymbol{X}}$. Even if for experimental scientists it may be more convenient to analyze elastic domain shape through the observable stress tensor $\boldsymbol{\sigma}$, the generalized force $\boldsymbol{X}$ portrayal has one conceptual advantage in thermodynamics. Indeed, as we have seen in (2.5), the generalized force appears to be a natural variable in the dissipation rate function.

It is clear that to get a complete material description, the plastic variable evolution $\dot{\boldsymbol{p}}$ needs to be introduced. This is commonly done either through a dissipation potential [14], a plastic potential [41] or directly via an explicit flow rule. For an arbitrary flow rule, the proof of the positiveness of the dissipation rate (2.5) is a rather challenging task. But if the plastic strain rate depends exclusively on generalized plastic force ($\dot{\boldsymbol{p}} \Leftrightarrow \boldsymbol{X}$), the material dissipation rate becomes an exclusive function of generalized force $\mathcal{D} = \mathcal{D}(\boldsymbol{X})$. This is some supplementary restrictive hypothesis, but in this case, the positivity of dissipation is automatically independent of the loading path: it is a combination of the geometrical properties of the elastic domain shape and the functional properties of a flow rule. The whole model can be then analyzed in the generalized forces space, which is the basis of Standard Generalized Material formalism [14]. We adopt the latter formalism in the current paper in order to detail an example of complete constitutive relation (section 3) derived from the main considerations presented in the next subsection.

2.3 Main idea in the nutshell

Among the many possible extensions of the basic perfect plasticity constitutive model, we are interested in plastic-to-hyperelastic coupling. To derive the main conclusions we need four assumptions that have been discussed earlier in this section, i.e., we suppose that:

- the current state is defined by two state variables: the total infinitesimal strain $\boldsymbol{\varepsilon}$ and the plastic strain $\boldsymbol{p}$;
- the evolution relies on Helmholtz free energy $\phi(\boldsymbol{\varepsilon}, \boldsymbol{p})$, i.e. $\boldsymbol{\sigma} = \partial\phi/\partial\boldsymbol{\varepsilon}$ and $\boldsymbol{X} = -\partial\phi/\partial\boldsymbol{p}$;
- the elastic domain is defined in the space of generalized plastic force $\boldsymbol{X}$;
- the strain-stress relation is nonlinear during unloading;

Remark 1 (Flow rule choice). At this stage, as we have no intention to analyze the full model response, it is not necessary to make any flow rule choice. This choice will indeed be crucial in the next section.

We focus first on the yield surface modification generated by the presence of nonlinear elasticity. For geomaterials (like rocks, clays, soils, etc.), the reversible elastic domain is

comparatively small and is usually of hysteretical nature, so it is hard to quantify experimentally. With missing experimental data, it is not surprising to find most industrial modeling admitting linear elastic domain approximation. Nevertheless, some recent well-documented experiments manage to separate and evaluate the elastic nonlinearity itself. For example, in [23] the authors conducted local cyclic loadings on sand underlying its hyperelastic properties. Even if this new experiment sheds light on this longtime neglected phenomenon, the general hyperelastic coupling term is too complex to be fully identified. Natural questions arise on how to handle all possible couplings in the multidimensional tensor relation. In this article, it is shown that the hyperelastic coupling term can be simplified (see (2.8)) enabling its analysis with the currently accessible experimental databases (e.g. [23]).

Nonlinear elasticity may be introduced in many different ways by alternating the most simple quadratic free energy form (2.2). We consider here one of its possible extensions, where the elastic modulus is supposed to be some function of the total strain, i.e., $\mathbb{E} = \mathbb{E}(\boldsymbol{\varepsilon})$, while the quadratic term involving $\boldsymbol{\varepsilon} - \boldsymbol{p}$ is maintained:

$$\phi(\boldsymbol{\varepsilon}, \boldsymbol{p}) = \frac{1}{2}\mathbb{E}(\boldsymbol{\varepsilon})(\boldsymbol{\varepsilon} - \boldsymbol{p})^2. \tag{2.6}$$

The stress-strain relationship becomes as expected nonlinear, but more than that *the stress is no longer equal to the generalized plastic force*:

$$\boldsymbol{X} = \mathbb{E}(\boldsymbol{\varepsilon})(\boldsymbol{\varepsilon} - \boldsymbol{p}) \neq \boldsymbol{\sigma}.$$

Formal writing of the expression for the stress gives:

$$\boldsymbol{\sigma} = \mathbb{E}(\boldsymbol{\varepsilon})(\boldsymbol{\varepsilon} - \boldsymbol{p}) + \frac{\partial \mathbb{E}}{2\partial \boldsymbol{\varepsilon}}(\boldsymbol{\varepsilon} - \boldsymbol{p})^2 = \boldsymbol{X} + \frac{\partial \mathbb{E}}{2\mathbb{E}(\boldsymbol{\varepsilon})^2 \partial \boldsymbol{\varepsilon}}\boldsymbol{X}^2. \tag{2.7}$$

In general, if the elastic domain is fixed in the space of generalized force $\boldsymbol{X}$, in the presence of hyperelasticity it becomes strain-dependent in the space of stresses $\boldsymbol{\sigma}$. They will be denoted with $\mathbb{K}_{\boldsymbol{X}}$ and $\mathbb{K}_{\boldsymbol{\sigma}}$, respectively. Notice that this is also what happens in the case we are considering. Indeed, for small loading ($\boldsymbol{X} \ll 1$) the quadratic term $\sim \boldsymbol{X}^2$ could be considered as a nonlinear kinematic hardening, but in general the equation (2.7) states the nonlinear modification of the initial elastic domain, i.e., $\mathbb{K}_{\boldsymbol{\sigma}} \neq \mathbb{K}_{\boldsymbol{X}}$. For the cyclic loading, the initial yield surface is modified on each back-and-forth loop creating a mechanism similar to those introduced earlier by different authors, like the bounding surface in [6] or parent/child surfaces like in Hujeux constitutive relation [2]. Therefore, in the current formulation, *the presence of nonlinear hyperelasticity in plastic materials introduces not only a nonlinear stress-strain relationship but also affects the elastic domain shape making it loading-dependent in stress space.* The hyperelasticity is seen as model enrichment for the whole set of loading and not only for reversible ones. As a consequence, the post-pic behavior may be used to fit hyperelastic parameters and viceversa, completing experimental data.

While all previously cited advantages of our particular formalism for nonlinear elasto-plasticity are up to now hypothetical, the attentive reader may remark that hyperelasticity coupling function $\mathbb{E}(\boldsymbol{\varepsilon})$ is still too complex to be fitted experimentally. Anticipating this remark, we proceed further and *introduce a particular class of hyperelasto-plastic materials that have fixed yield criterion in the stress space.* This yield criterion can be considered either as initial elastic domain or as residual yield surface, for example for fully damaged elasto-plastic coupled to damage behavior [30]. As the elastic domain in the space of

generalized force $\boldsymbol{X}$ is supposed to be fixed, it would also stay fixed in the space of stresses $\boldsymbol{\sigma}$ if and only if the coupling term in (2.7) is constant:

$$\frac{\partial \mathbb{E}}{2\mathbb{E}^2 \partial \boldsymbol{\varepsilon}} = \text{const}.$$

This condition defines one particular class of hyperelastic materials that keep the elastic domain $\mathbb{K}_{\boldsymbol{\sigma}}$ fixed. This equation states that the material compliance should be linear with total strain:

$$\frac{\partial \mathbb{E}}{2\mathbb{E}^2 \partial \boldsymbol{\varepsilon}} = -\frac{\partial \mathbb{E}^{-1}}{2\partial \boldsymbol{\varepsilon}} = \text{const} \qquad \Longrightarrow \qquad \mathbb{E}^{-1} \sim \boldsymbol{\varepsilon}. \tag{2.8}$$

This formal writing of a tensor-based expression is certainly over-simplified, but it allows us to propose a subclass of hyperelastic materials that have a fixed yield surface in the stress space. We will show in the next section, that this condition can be reached for instance by setting both Lamé coefficients as hyperbolic functions of the strain trace.

Coming back to the nonlinear relation (2.7) with hyperbolic constrain, we remark that it simplifies to the straight quadratic mapping: $\boldsymbol{\sigma} = \boldsymbol{X} + \beta \boldsymbol{X}^2$, with $\beta = \text{const}$. If the subsequent constitutive relation is obtained under the assumptions of Standard Generalized Materials [14, 9], this last expression may be considered as a transformation of the thermodynamic reversible domain in the generalized forces space $\boldsymbol{X}$ to the experimentally observable elastic domain in the stress space $\boldsymbol{\sigma}$. It is then intuitively clear that the model constructed starting from a linear plasticity criterion in the generalized force space (Drucker–Prager type in $\boldsymbol{X}$) will lead to a nonlinear elastic constitutive law with a quadratic domain in the stress space (Hoek–Brown type in $\boldsymbol{\sigma}$). In some sense, the Hoek–Brown is nothing else than a nonlinear version of the Drucker–Prager.

3 Hyperelastic enrichment of perfect plasticity

As it was announced shortly above, in this section we display how to derive the elasto-plastic constitutive relation with a three-dimensional Hoek–Brown type yield surface starting from the model with linear plastic criterion in the case of the hyperbolic elasticity.

Above and throughout this section, we use the usual notation of mechanics: $\boldsymbol{u}$ is the unknown displacement field, $\boldsymbol{\varepsilon} \in \mathbb{R}^{3\times3}_{\text{sym}}$ is the strain tensor, i.e., the symmetric part of the gradient of $\boldsymbol{u}$, $\boldsymbol{p} \in \mathbb{R}^{3\times3}_{\text{sym}}$ is the plasticity component of the strain tensor, i.e., $\boldsymbol{p} = \boldsymbol{\varepsilon} - \boldsymbol{\varepsilon}^{\text{el}}$, $\boldsymbol{\sigma} \in \mathbb{R}^{3\times3}_{\text{sym}}$ is the stress tensor, and $\boldsymbol{X} \in \mathbb{R}^{3\times3}_{\text{sym}}$ is the thermodynamical force associated with plasticity, i.e., the plastic dual variable. Strain and plasticity tensors are the state variables of our model and, for simplicity, they are decomposed into their volumetric and deviatoric parts:

$$\boldsymbol{\varepsilon} = \frac{1}{3}\operatorname{Tr}\boldsymbol{\varepsilon}\,\mathbf{I}_2 + \boldsymbol{\varepsilon}^D \qquad \text{and} \qquad \boldsymbol{p} = \frac{1}{3}\operatorname{Tr}\boldsymbol{p}\,\mathbf{I}_2 + \boldsymbol{p}^D.$$

where, as before, we note $\mathbf{I}_2$ as second-order identity tensor. These expressions can be used as zero trace tensor deviator definition: $\operatorname{Tr}\boldsymbol{\varepsilon}^D = 0$ and $\operatorname{Tr}\boldsymbol{p}^D = 0$. We adopt the usual convention in Mechanics of Continuous Media for the sign of strain and stress, i.e., the stress is positive in traction and negative in compression.

3.1 Brief history of quadratic yield criteria

We start first with a brief description of the history of the introduction of quadratic yield surfaces, what we call "Hoek–Brown-type" yield surfaces.

Back in 1924, while studying the mechanical behavior of glasses, Griffith [13] was the first to derive from theoretical considerations a quadratic multi-axial criterion for fracture:

$$(\sigma_1 - \sigma_3)^2 \sim (\sigma_1 + \sigma_3)$$

where σ_1 and σ_3 are the major and minor principal stresses, respectively.
Forty years later, Fairhurst [10] attempted to empirically extend the work of Griffith to the domain of high compression suitable for rock behavior analysis. Finally, in 1980 Hoek and Brown [16] obtained a criterion shape that convinced many generations of geomaterial scientists. The original Hoek–Brown criterion is still widely used in rock mechanics and, for intact rocks, it can be written as:

$$\sigma_1 = \sigma_3 + C_0\sqrt{m_i\frac{\sigma_3}{C_0} + 1},$$

where C_0 is the uniaxial compressive strength and m_i is a material constant for the intact rock. For more details about these constants, we refer to [18], where a generalized version of the criterion involving the geological strength index (GSI) is also proposed and analyzed. Furthermore, the evolution of the Hoek–Brown criterion in the literature is summarized in the article [19].

Since many papers have exhibited the strong influence of the intermediate principal stress σ_2 (see, e.g., [27, 8] and the references therein), different three-dimensional extensions based on the Hoek–Brown criterion has been developed [35, 42, 36, 27]. In particular, its generalized form written with the help of rotational invariants was proposed by X. D. Pan and J. Hudson [34]. For intact rocks, it reads as:

$$\frac{3}{2C_0}\left\|\boldsymbol{\sigma}^D\right\|^2 + \frac{\sqrt{3}m_{\mathrm{i}}}{2\sqrt{2}}\left\|\boldsymbol{\sigma}^D\right\| + m_{\mathrm{i}}\sigma_m - C_0 = 0,$$

where σ_m and $\boldsymbol{\sigma}^D$ are the spherical and deviatoric parts of the stress tensor, respectively, i.e.,

$$\boldsymbol{\sigma} = \sigma_m\,\mathbf{I}_2 + \boldsymbol{\sigma}^D, \qquad \text{where } \sigma_m = \frac{1}{3}\mathrm{Tr}\,\boldsymbol{\sigma}, \tag{3.1}$$

and $\left\|\boldsymbol{\sigma}^D\right\| := \sqrt{\boldsymbol{\sigma}^D : \boldsymbol{\sigma}^D}$, it is usually called second deviator stress invariant J_2 in geotechnical industry. Here, the double dot product is simply the double contraction operation for second-order tensors. All the described criteria are parabolic and can be summarized as various choices of constants in the general expression:

$$f_{\boldsymbol{\sigma}} = A\left\|\boldsymbol{\sigma}^D\right\|^2 + B\left\|\boldsymbol{\sigma}^D\right\| + C\sigma_m - D = 0.$$

In this article, we don't suppose but derive a quadratic yield criterion of this type under the assumption of Standard Generalized Materials [14] in a variational framework in the presence of hyperelasticity. In particular, as we have already mentioned, we will show that this model can be constructed by starting from an elasto-plastic model with a Drucker–Prager (linear) plasticity criterion and introducing hyperbolic hyperelastic dependence in some material parameters. This will lead to a nonlinear elastic constitutive relation with Hoek–Brown (quadratic) type yield surface.

3.2 Mapping thermodynamics to observables

In this section, we propose one specific form of the energy density that realized the (2.8) condition and derive then the stress tensor expression as a function of generalized forces. We begin our analysis by specifying the free energy density for the perfect elasto-plastic model (2.2), which corresponds to the non-hardening version of [30, Equation (11)], where the material is assumed to be isotropic:

$$\begin{aligned}\phi(\boldsymbol{\varepsilon},\boldsymbol{p}) &= \frac{1}{2}\mathbb{E}(\boldsymbol{\varepsilon}-\boldsymbol{p}):(\boldsymbol{\varepsilon}-\boldsymbol{p})\\ &= \frac{1}{2}K(\operatorname{Tr}\boldsymbol{\varepsilon}-\operatorname{Tr}\boldsymbol{p})^2+\mu(\boldsymbol{\varepsilon}^D-\boldsymbol{p}^D):(\boldsymbol{\varepsilon}^D-\boldsymbol{p}^D).\end{aligned} \tag{3.2}$$

Here, the action of the fourth order elasticity tensor $\mathbb{E}$ is described by $\mathbb{E}\boldsymbol{\tau}=\lambda\operatorname{Tr}\boldsymbol{\tau}\,\mathbf{I}_2+2\mu\boldsymbol{\tau}$ for any second order tensor $\boldsymbol{\tau}$, $\lambda>0$ is the Lamé parameter, $\mu>0$ is the shear modulus, and $K=\lambda+{}^{2\mu}/_{3}$ is the compressibility modulus of the material. The dual variables $\boldsymbol{\sigma}$ and $\boldsymbol{X}$ can be obtained by deriving the energy density (3.2) with respect to the state variables $\boldsymbol{\varepsilon}$ and $\boldsymbol{p}$:

$$\boldsymbol{\sigma}\coloneqq\frac{\partial\phi}{\partial\boldsymbol{\varepsilon}}(\boldsymbol{\varepsilon},\boldsymbol{p}) \qquad \text{and} \qquad \boldsymbol{X}\coloneqq-\frac{\partial\phi}{\partial\boldsymbol{p}}(\boldsymbol{\varepsilon},\boldsymbol{p}). \tag{3.3}$$

Within current thermodynamic formalism, this equation may be considered as a definition, which is why we are using the $\coloneqq$ sign. In particular, we recall that in this case we simply obtain (2.3).

Now, we introduce some hyperelasticity dependencies in the elasticity tensor, and, in particular, we suppose $\mathbb{E}=\mathbb{E}(\operatorname{Tr}\boldsymbol{\varepsilon})$. If trace dependence is natural, the deviator one is not obvious, as it wouldn't be derivable on the hydrostatic axis. Here, we meet the required condition (2.8) by assuming the following hyperbolic relations:

$$K(\operatorname{Tr}\boldsymbol{\varepsilon})=\frac{K_i}{2K_i\beta_m\operatorname{Tr}\boldsymbol{\varepsilon}+1} \qquad \text{and} \qquad \mu(\operatorname{Tr}\boldsymbol{\varepsilon})=\frac{\mu_i}{4\mu_i\beta^D\operatorname{Tr}\boldsymbol{\varepsilon}+1}, \tag{3.4}$$

where $K_i>0$ and $\mu_i>0$ are the sound material's initial compressibility and shear moduli, $\beta_m\geq 0$ and $\beta^D\geq 0$ are the hyperelastic parameters of the model. In addition, we restrict ourselves to the tests in which

$$\operatorname{Tr}\boldsymbol{\varepsilon}>\varepsilon_0\coloneqq\max\left\{-\frac{1}{2K_i\beta_m},-\frac{1}{4\mu_i\beta^D}\right\} \tag{3.5}$$

in order to ensure the positivity of $K_0(\operatorname{Tr}\boldsymbol{\varepsilon})$ and $\mu_0(\operatorname{Tr}\boldsymbol{\varepsilon})$. Denoting with X_m and $\boldsymbol{X}^D$ the spherical and deviatoric components of $\boldsymbol{X}$ as we have done for the stress (3.1), the expression of $\boldsymbol{\sigma}$ and $\boldsymbol{X}$ can be easily obtained thanks to (3.3):

$$\begin{cases}\sigma_m=\dfrac{K_i}{2K_i\beta_m\operatorname{Tr}\boldsymbol{\varepsilon}+1}(\operatorname{Tr}\boldsymbol{\varepsilon}-\operatorname{Tr}\boldsymbol{p})-\dfrac{K_i^2\beta_m}{(2K_i\beta_m\operatorname{Tr}\boldsymbol{\varepsilon}+1)^2}(\operatorname{Tr}\boldsymbol{\varepsilon}-\operatorname{Tr}\boldsymbol{p})^2\\ \qquad\quad -\dfrac{4\mu_i^2\beta^D}{(4\mu_i\beta^D\operatorname{Tr}\boldsymbol{\varepsilon}+1)^2}(\boldsymbol{\varepsilon}^D-\boldsymbol{p}^D):(\boldsymbol{\varepsilon}^D-\boldsymbol{p}^D),\\ \boldsymbol{\sigma}^D=\dfrac{2\mu_i}{4\mu_i\beta^D\operatorname{Tr}\boldsymbol{\varepsilon}+1}(\boldsymbol{\varepsilon}^D-\boldsymbol{p}^D),\end{cases} \tag{3.6}$$

and

$$\begin{cases}X_m=\dfrac{K_i}{2K_i\beta_m\operatorname{Tr}\boldsymbol{\varepsilon}+1}(\operatorname{Tr}\boldsymbol{\varepsilon}-\operatorname{Tr}\boldsymbol{p}),\\ \boldsymbol{X}^D=\dfrac{2\mu_i}{4\mu_i\beta^D\operatorname{Tr}\boldsymbol{\varepsilon}+1}(\boldsymbol{\varepsilon}^D-\boldsymbol{p}^D).\end{cases} \tag{3.7}$$

As a consequence, $\boldsymbol{\sigma}$ and $\boldsymbol{X}$ are connected through the following relation:

$$\boldsymbol{\sigma} = \boldsymbol{X} - \left(\beta_m X_m^2 + \beta^D \boldsymbol{X}^D : \boldsymbol{X}^D\right) \mathbf{I}_2. \tag{3.8}$$

The hyperbolic nonlinearity (3.4) generates quadratic stress $\boldsymbol{\sigma}$ to generalized forces $\boldsymbol{X}$ relation, that does not depend on plastic criterion. It only involves the hyperelastic parameters β_m and β^D. The relation is bijective ($\boldsymbol{\sigma} \Leftrightarrow \boldsymbol{X}$) and easily invertible. If we remark that $\boldsymbol{X}^D = \boldsymbol{\sigma}^D$ the implicit relation for the hydrostatic part reads:

$$X_m - 3\beta_m X_m^2 = \sigma_m + 3\beta^D \boldsymbol{\sigma}^D : \boldsymbol{\sigma}^D. \tag{3.9}$$

As expected, equation (3.9) preserves eigenspace decomposition, which allows in principle to establish a full continuously derivable relation between all three eigenvalues for stresses $\boldsymbol{\sigma}$ and generalized forces $\boldsymbol{X}$. Some general domain transformation properties can be claimed:

- all domains may be represented in 3D eigenvalue space
- bounded/unbounded domain property is transformation invariant
- domain boundary singularities are preserved: 2D edge to edge or 1D vertex to vertex
- hydrostatic axis rotational symmetry is transformation invariant

For the particular case of $\beta^D = 0$ the transformation is equivalent to a quadratic rescaling of the hydrostatic axis, that preserves deviatoric clipping plane shapes. In this case, it is clear that Mohr–Coulomb cone with hexagonal cross-section in the deviatoric plane will be transformed to some extension of the Hoek–Brown criterion characterized by one singularity on the hydrostatic axis, hexagonal cross-section in the deviatoric plane, quadratic profile for any hydrostatic plane cut.

Once again, as we have pointed out earlier in the previous section, the nonlinear relation (3.8) may be considered as a transformation rule of the thermodynamically defined reversible domain to the experimentally observable elastic domain. In fact, any shape set in generalized forces $\boldsymbol{X}$ (thermodynamic one) has a one-to-one map to its counterpart in the observable stress space $\boldsymbol{\sigma}$ (experimental one). Our general observation is that the nonlinearity in elasticity influences the thermodynamic-to-experimental mapping of the reversible domain. Even if in itself it seems to open a vast investigation field, in this paper we focus mainly on the most simple example of Drucker–Prager criteria transformation, which is detailed in the following section.

3.3 The plasticity criterion transformation

As it was said just above, we consider here the most simple, the Drucker–Prager criterion transformation by hyperelastic coupling. In the $\boldsymbol{X}$–space it reads:

$$f_{\boldsymbol{X}}(\boldsymbol{X}) \coloneqq \frac{1}{\sqrt{6}} \left\|\boldsymbol{X}^D\right\| + aX_m - b = 0, \tag{3.10}$$

where $a > 0$ and $b \geq 0$, and we recall that $\|\boldsymbol{\tau}\| \coloneqq \sqrt{\boldsymbol{\tau} : \boldsymbol{\tau}}$. The corresponding elastic domain $\mathbb{K}_{\boldsymbol{X}} \coloneqq \{\boldsymbol{X}^* \in \mathbb{R}^{3\times3}_{\text{sym}} : f_{\boldsymbol{X}}(\boldsymbol{X}^*) \leq 0\}$ is a convex cone with a singular point at $(b/a, \mathbf{0})$, and the behavior remains elastic while $f_{\boldsymbol{X}}(\boldsymbol{X}) < 0$. Moreover, in order to satisfy the positivity of dissipation condition (2.5) [14], consistently with the Standard

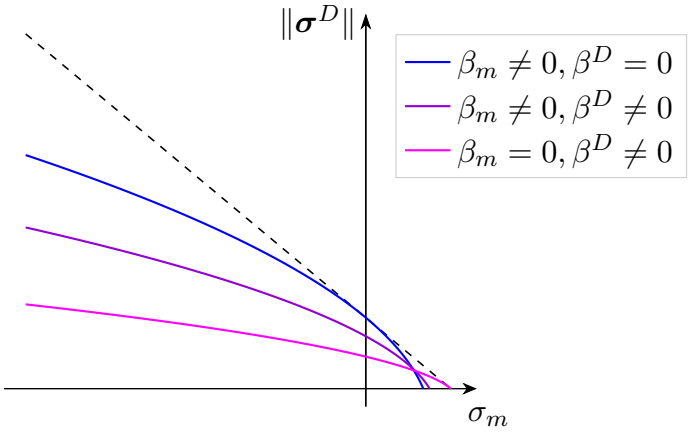

Figure 1: Transformation of the failure criterion for different values of the hyperelastic coefficients β_m and β^D. The black dashed line represents the degenerated case (i.e.$\beta_m = \beta^D = 0$) of linear failure criterion (3.14), that is equivalent to the initial one (3.10).

Generalized Materials framework, we consider an associative model, i.e., we assume that the plasticity evolution follows the normality rule. As a consequence, in the points in which the boundary is smooth, i.e., where the function $f_{\boldsymbol{X}}$ is differentiable, we have

$$\dot{\boldsymbol{p}} = \dot{\lambda}\left(\frac{1}{\sqrt{6}}\frac{\boldsymbol{X}^D}{\|\boldsymbol{X}^D\|} + \frac{a}{3}\mathbf{I}_2\right), \qquad \dot{\lambda} \geq 0. \tag{3.11}$$

For further details, we refer the reader to [30, Section 2]. In addition, if $b \neq 0$, we assume

$$\beta_m \leq \frac{a}{2b}. \tag{3.12}$$

Combining (3.10) with (3.8), one can obtain the explicit expression of the plasticity criterion in the stress space:

$$f_{\boldsymbol{\sigma}}(\boldsymbol{\sigma}) \coloneqq \frac{1}{6}\left(\beta_m + 6a^2\beta^D\right)\left\|\boldsymbol{\sigma}^D\right\|^2 + \frac{1}{\sqrt{6}}\left(a - 2\beta_m b\right)\left\|\boldsymbol{\sigma}^D\right\| + a^2\sigma_m - b\left(a - \beta_m b\right) = 0. \tag{3.13}$$

Therefore, starting from the linear failure criterion (3.10) for the generalized force $\boldsymbol{X}$, we obtain a quadratic failure criterion for the stress tensor $\boldsymbol{\sigma}$. The corresponding reversibility domain $\mathbb{K}_{\boldsymbol{\sigma}} \coloneqq \{\boldsymbol{\sigma}^* \in \mathbb{R}^{3\times3}_{\text{sym}} \,:\, f_{\boldsymbol{\sigma}}(\boldsymbol{\sigma}^*) \leq 0\}$ is a convex cone with parabolic boundary and a singular point in $\left(\frac{b(a-\beta_m b)}{a^2}, \mathbf{0}\right)$. Notice that, since (3.13) does not depend on $\boldsymbol{\varepsilon}$ or $\boldsymbol{p}$, $\mathbb{K}_{\boldsymbol{\sigma}}$ remains fixed for any type of evolution. Figure 1 shows the transformation of the failure criterion from linear to quadratic for three different choices of the hyperelasticity parameters (β_m, β^D).

Remark 2 (Motivations of assumption (3.12)). Assumption (3.12) ensures that the domain in the stress space is convex and contains the origin $\mathbf{0}$ of the space. Furthermore, with this condition, the quadratic failure criterion can be written as

$$\frac{1}{\sqrt{6}}\left\|\boldsymbol{\sigma}^D\right\| = \frac{-(a - 2\beta_m b) + a\sqrt{1 - 4\sigma_m(\beta_m + 6a^2\beta^D) + 24\beta^D b(a - \beta_m b)}}{2(\beta_m + 6a^2\beta^D)}.$$

The classical linear Drucker–Prager expression is naturally recovered for vanishing hyperelastic coupling, i.e. for $\beta_m = \beta^D = 0$:

$$\frac{1}{\sqrt{6}} \left\| \boldsymbol{\sigma}^D \right\| = b - a\sigma_m. \tag{3.14}$$

We see from Figure 1 that (a, b) plays the role of friction-cohesion coefficient's pair defining linear domain that envelopes the final elastic shape (3.13) for any hyperelastic coupling coefficients $\beta_m \cdot \beta^D \neq 0$.

To summarize, we have shown in this section different possible transformations of the linear Drucker–Prager cone to a quadratic Hoek–Brown's one generated by the hyperelastic coupling.

4 Response on typical tests

The aim of this section is to show a panel of examples of evolution using the proposed hyperelastic model in some typical test cases. In particular, we want to exhibit the influence of the hyperelastic parameters and provide a comparison with the linear elasto-plastic model. The results are obtained with the open source code generation tool `mfront` (see [15] and also `http://tfel.sourceforge.net`). For all tests, we start from a natural reference configuration with $\boldsymbol{p} = \mathbf{0}$, and we set the Poisson's ratio $\nu = 0.3$, which corresponds to the compressibility modulus $K_i = 5E/6$ and to the shear modulus $\mu_i = 5E/13$. Apart from these elastic coefficients, we need to define a pair of linear domain parameters that are equivalent to the classical frictional and cohesive one a, b and one more pair of the hyperelastic coefficients β_m, and β^D.

In the preliminary analysis, one may be interested in the investigation of the elastic response for small loading. Some relevant information for model parameter identification can be extracted from (3.6) for $\operatorname{Tr}\boldsymbol{\varepsilon} \ll \varepsilon_0$ at the initial stage $\boldsymbol{p} = 0$. It shows, first, that Poisson's ratio and Young modulus preserve their classical meaning, and second, that the deviatoric hyperelastic coefficient β^D couples the volumetric stress σ_m to deviatoric strain for pure deviatoric loading, i.e. for $\operatorname{Tr}\boldsymbol{\varepsilon} = 0$. Finally, for the identification of the hyperelastic coefficient β_m one may need to go over the linear elastic response, but it can be also fitted experimentally straight from the hydrostatic response, for example from the strain compression limit ε_0 (see next subsection). Consequently, all elastic and hyperelastic parameters can be identified by a subtle analysis of elastic response. We study quantitatively all the relations in the next subsections.

4.1 Hydrostatic tests

During a hydrostatic test, the stress remains on the hydrostatic axis throughout the loading. This corresponds to the assumption that only the spherical part of the stress evolves, i.e., $\boldsymbol{\sigma} = \bar{\sigma}\mathbf{I}_2$, with $\bar{\sigma} < 0$ for compression tests, and $\bar{\sigma} > 0$ for traction tests. We recall that the compression limit is fixed, either by β_m or β_D (see (3.5)). Here for simplicity we suppose that $K_i\beta_m \geq 2\mu_i\beta^D$ so that $\varepsilon_0 = -\dfrac{1}{2K_i\beta_m}$. Consequently, it's a β_m that defines the hydrostatic compression limit. From the second equation of (3.6), we have immediately that $\boldsymbol{\varepsilon}^D = \mathbf{0}$. Therefore, using the first equation of (3.6), we recover that for hydrostatic loading when the behavior is hyperelastic, i.e., $\boldsymbol{\sigma} \in \operatorname{Int}\mathbb{K}_{\boldsymbol{\sigma}}$, the evolution is

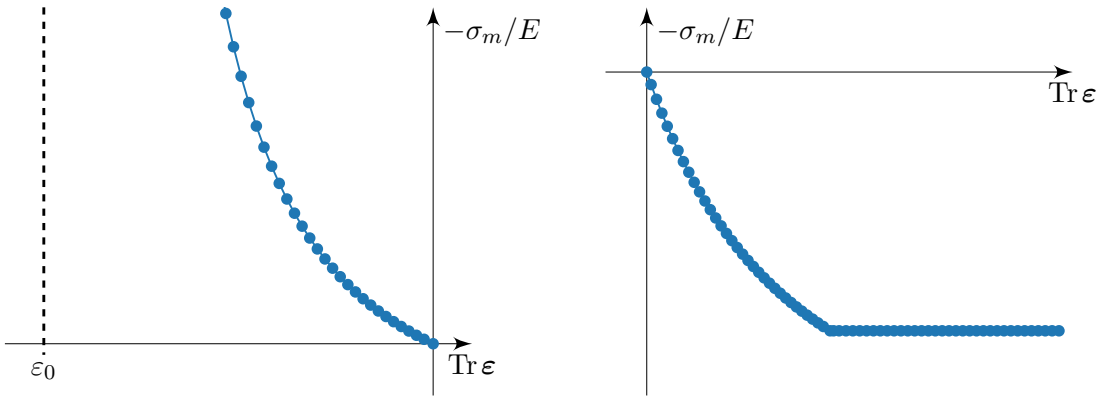

Figure 2: Graphs of hydrostatic triaxial test: compression (*left*) and traction (*right*).

simply described by

$$\boldsymbol{\sigma} = \sigma_m \mathbf{I}_2 = \left[\frac{K_i}{2K_i\beta_m \mathrm{Tr}\,\boldsymbol{\varepsilon} + 1} \mathrm{Tr}\,\boldsymbol{\varepsilon} - \frac{K_i^2 \beta_m}{(2K_i\beta_m \mathrm{Tr}\,\boldsymbol{\varepsilon} + 1)^2} (\mathrm{Tr}\,\boldsymbol{\varepsilon})^2 \right] \mathbf{I}_2, \tag{4.1}$$

or

$$\boldsymbol{\varepsilon} = \frac{\mathrm{Tr}\,\boldsymbol{\varepsilon}}{3} \mathbf{I}_2 = \left[\frac{1}{6K_i\beta_m} \left(-1 + \frac{1}{\sqrt{1 - 4\beta_m\sigma_m}} \right) \right] \mathbf{I}_2. \tag{4.2}$$

This is the case for any value of hydrostatic compression and for the first part of hydrostatic traction. More in detail, in a traction test, initially the behavior is hyperelastic until σ_m reaches its maximum value determined by the plasticity criterion (3.13): $\dfrac{b(a - \beta_m b)}{a^2}$. Then, the spherical part of the stress remains constant and plasticity evolves. One can see the corresponding graphs of the evolution of the hydrostatic stress σ_m as a function of $\mathrm{Tr}\,\boldsymbol{\varepsilon}$ in Figure 2, in the case of compression (*left*) and traction (*right*) with parameters $a = 1$, $b = E/1000$, $\beta_m = 200/E$, and any $\beta^D \leq 13\beta_m/12$. We notice that even if the plots are shown separately, for all $b > 0$, the transition between compression/traction is continuous and differentiable since it is described by the regular in the interval $(\varepsilon_0; \infty)$ function (4.1).

As we have observed earlier in this section, β_m may be fitted experimentally straight from the hydrostatic compression limit ε_0. Provided the β_m coefficient is known from this preliminary elastic analysis in compression, the hydrostatic loading in the opposite direction gives us access to the tensile strength limit, meaning in practice to experimentally fit the a to b ratio (one of the relations defining the criterion shape). While the solicitations are mostly elastic, the domain shape cannot be precisely identified and a second experimental setup is needed. In the next subsection, we propose to study a triaxial compression, that allows full model parameter identification by solicitation of another mixed-loading plasticity limit.

4.2 Triaxial compression test with a confining pressure

A triaxial compression test with a confining pressure is divided into two phases:

- at first, a hydrostatic compression is performed reaching the value of pressure $p_0 > 0$,
- then, we compress along the z–axis maintaining the lateral pressure constant.

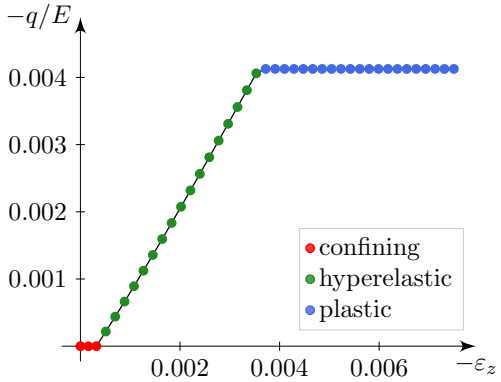

(a) Deviatoric stress $q = \sigma_x - \sigma_z$ vs. axial strain ε_z.

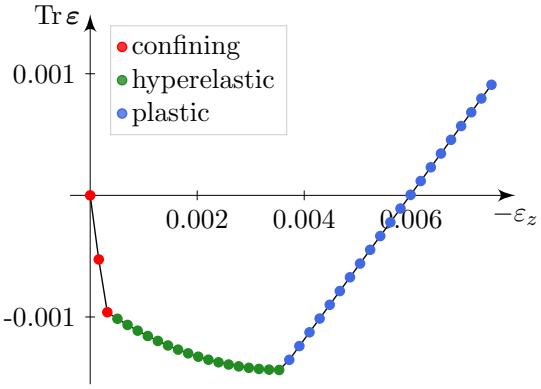

(b) Volumetric strain $\mathrm{Tr}\,\boldsymbol{\varepsilon}$ vs. axial strain ε_z.

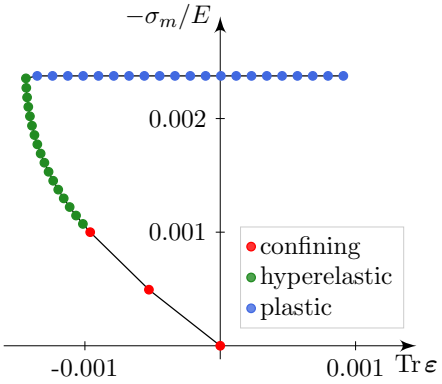

(c) Average stress σ_m vs. volumetric strain $\mathrm{Tr}\,\boldsymbol{\varepsilon}$.

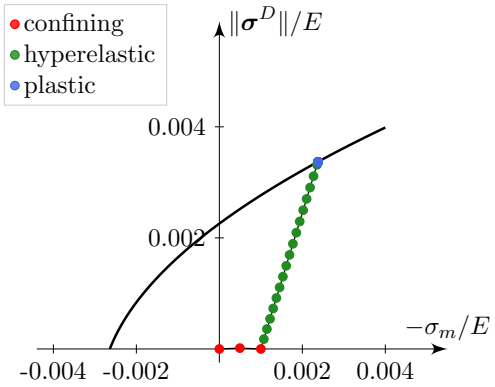

(d) Evolution in the stress domain.

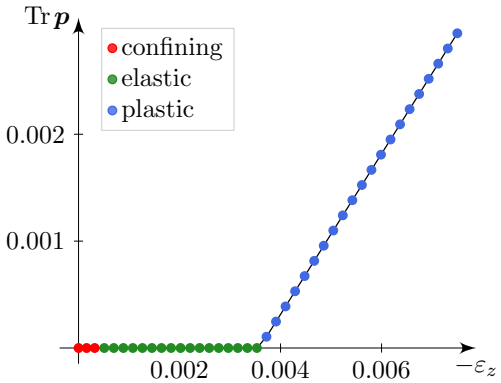

(e) Volumetric plastic strain $\mathrm{Tr}\,\boldsymbol{p}$ vs. axial strain ε_z.

Figure 3: Graphs of triaxial compression test with a confining pressure. The different stages of the evolution are shown with different colors: hydrostatic confining (*red*), hyperelastic (*green*), and plastic (*blue*) stage.

As we have already seen in the previous subsection, during the confining phase the behavior is (nonlinear) elastic, i.e., $\boldsymbol{p} = \mathbf{0}$, and only the hydrostatic component evolves, i.e., $\boldsymbol{\sigma}^D = \boldsymbol{\varepsilon}^D = \mathbf{0}$. In addition, the evolution is determined by (4.1). At the end of this stage $\boldsymbol{\sigma} = -p_0\,\mathbf{I}_2$ and $\boldsymbol{\varepsilon} = \bar{\varepsilon}\,\mathbf{I}_2$, where $\bar{\varepsilon}$ can be found out thank to (4.2):

$$\bar{\varepsilon} \coloneqq \frac{1}{6K_i\beta_m}\left(-1 + \frac{1}{\sqrt{4\beta_m p_0 + 1}}\right).$$

Then, during the second phase of the loading, we prescribe the evolution of ε_z with $\dot{\varepsilon}_z < 0$, while the lateral pressure stays equal to p_0:

$$\boldsymbol{\sigma} = \begin{pmatrix} -p_0 & 0 & 0 \\ 0 & -p_0 & 0 \\ 0 & 0 & \sigma_z \end{pmatrix} \qquad \text{and} \qquad \boldsymbol{\varepsilon} = \begin{pmatrix} \varepsilon_x & 0 & 0 \\ 0 & \varepsilon_x & 0 \\ 0 & 0 & \varepsilon_z \end{pmatrix}.$$

In particular, we have

$$\sigma_m = \frac{1}{3}(\sigma_z - 2p_0) \qquad \text{and} \qquad \|\boldsymbol{\sigma}^D\| = \sqrt{\frac{2}{3}}\,|p_0 + \sigma_z|, \tag{4.3}$$

and we define the deviatoric stress $q \coloneqq p_0 + \sigma_z$. Figure 3 shows the evolution curves for this kind of test with parameters given by:

$$a = \frac{1}{4}, \qquad b = \frac{E}{10^3}, \qquad \beta_m = \frac{85}{E}, \qquad \beta^D = \frac{60}{E}, \qquad p_0 = \frac{E}{10^3}. \tag{4.4}$$

In more detail, Figure 3a and 3b show the deviatoric stress q and the volumetric strain $\operatorname{Tr}\boldsymbol{\varepsilon}$ as functions of the axial strain ε_z, respectively, Figure 3c shows the spherical stress σ_m as a function of the volumetric strain $\operatorname{Tr}\boldsymbol{\varepsilon}$, and finally Figure 3d shows the evolution of the stress in the domain $\mathbb{K}_{\boldsymbol{\sigma}}$. After an initial elastic phase, the boundary of the reversibility domain $\mathbb{K}_{\boldsymbol{\sigma}}$ is reached, and, as a consequence, plasticity starts to evolve following the normality rule (3.11). The different stages of the evolution are highlighted with different colors in Figure 3: *red* for the confining stage, *green* for the hyperelastic stage, and *blue* for the stage with the progression of plasticity.

The nonlinear influence is evident during the hyperelastic phase (in *green*) in Figures 3b and 3c, whereas, as we can see in Figure 3d, the evolution inside the domain $\mathbb{K}_{\boldsymbol{\sigma}}$ remains linear. We can recover the explicit stress evolution expression for this elastic phase from (4.3):

$$\|\boldsymbol{\sigma}^D\| = -\sqrt{6}\,(\sigma_m + p_0). \tag{4.5}$$

During the plastic phase, the stress lies on the boundary of the elastic domain $\mathbb{K}_{\boldsymbol{\sigma}}$ and remains constant since there is no hardening, see Figure 3d. This point can be identified combining (4.5) with (3.13):

$$\begin{aligned} \boldsymbol{P}_1 &\coloneqq (\sigma_{1,m}, \|\boldsymbol{\sigma}_1^D\|) \\ &= \left(\frac{-2(\beta_m + 6a^2\beta^D)p_0 + a - 2\beta_m b - a^2 - \sqrt{\Delta_1}}{2(\beta_m + 6a^2\beta^D)}, -\sqrt{6}\,\frac{a - 2\beta_m b - a^2 - \sqrt{\Delta_1}}{2(\beta_m + 6a^2\beta^D)}\right), \end{aligned} \tag{4.6}$$

where

$$\Delta_1 := a^2(1-a^2) + 4(\beta_m + 6a^2\beta^D)(2+a)a\,p_0 + 4\beta_m a^2 b + 24\beta^D a^2 b(a - \beta_m b).$$

Figures 3a and 3c display the constant evolution of the average stress σ_m and the deviatoric stress q.

Finally, Figure 3b displays the presence of dilatancy without saturation, which is a consequence of the normal flow rule for the evolution of plasticity, see also Figure 3e. Indeed, during the plastic phase, inserting the first equation of (3.7) and the fact that $\boldsymbol{X}^D = \boldsymbol{\sigma}^D$ in (3.10), we have

$$\frac{1}{\sqrt{6}}\|\boldsymbol{\sigma}^D\| + a\frac{K_i}{2K_i\beta_m \operatorname{Tr}\boldsymbol{\varepsilon} + 1}(\operatorname{Tr}\boldsymbol{\varepsilon} - \operatorname{Tr}\boldsymbol{p}) - b = 0, \tag{4.7}$$

and then we achieve

$$\operatorname{Tr}\boldsymbol{\varepsilon} = \frac{\sqrt{6}\,a}{2\beta_m\|\boldsymbol{\sigma}^D\| + \sqrt{6}(a - 2b\beta_m)}\operatorname{Tr}\boldsymbol{p} + \frac{\sqrt{6}\,b - \|\boldsymbol{\sigma}^D\|}{K_i[2\beta_m\|\boldsymbol{\sigma}^D\| + \sqrt{6}(a - 2b\beta_m)]}.$$

We recall that $\|\boldsymbol{\sigma}^D\|$ is constant when the behavior is plastic.

Remark 3 (Analytical values of dilatancy). Combining the second equation of (3.6) with the flow rule (3.11) and (4.7), we get the analytical relation between the volumentric strain $\operatorname{Tr}\boldsymbol{\varepsilon}$ and the deviatoric strain $\varepsilon' := \varepsilon_x - \varepsilon_z$:

$$\operatorname{Tr}\boldsymbol{\varepsilon} = \frac{6a^2}{\sqrt{6}(\beta_m + 6a^2\beta^D)\|\boldsymbol{\sigma}^D\| + 3(a - 2b\beta_m)}\varepsilon' + C_1 =: L\varepsilon' + C_1, \tag{4.8}$$

where the constant C_1 depends on $\|\boldsymbol{\sigma}^D\|$ and on the parameters of the model. Observing that

$$\varepsilon' = \frac{\operatorname{Tr}\boldsymbol{\varepsilon}}{2} - \frac{3}{2}\varepsilon_z,$$

we obtain

$$\operatorname{Tr}\boldsymbol{\varepsilon} = -\frac{3L}{2-L}\varepsilon_z + C_2, \tag{4.9}$$

with C_2 constant and dependent only on $\|\boldsymbol{\sigma}^D\|$ and on the parameters of the model.

Remark 4 (Link between dilatancy and normal vector to $\mathbb{K}_{\boldsymbol{\sigma}}$). Consider the parabolic elastic domain $\mathbb{K}_{\boldsymbol{\sigma}}$. The vector

$$\left(\frac{6a^2}{\sqrt{6}(\beta_m + 6a^2\beta^D)\|\boldsymbol{\sigma}^D\| + 3(a - 2b\beta_m)}, \sqrt{\frac{2}{3}}\right)$$

is normal to the boundary of the domain in the point $(\sigma_m, \|\boldsymbol{\sigma}^D\|)$. Notice that the first component is exactly the linear term L that characterizes the slope of dilatancy, see (4.8) and (4.9).

To summarize under the triaxial compression we test the elastic domain limit for shear loading, this finally allows us to identify one missing model parameter. Precise expression depends on the analyzed behavior (either plastic limit (4.6) from Figures 3a and 3c, or dilatancy slope (4.9) from Figures 3b and 3e), but if this data is coupled with the initial hydrostatic test results all model parameters can be experimentally fitted, i.e. hyperelastic pair β_m and β^D, and the criterion shape pair a and b.

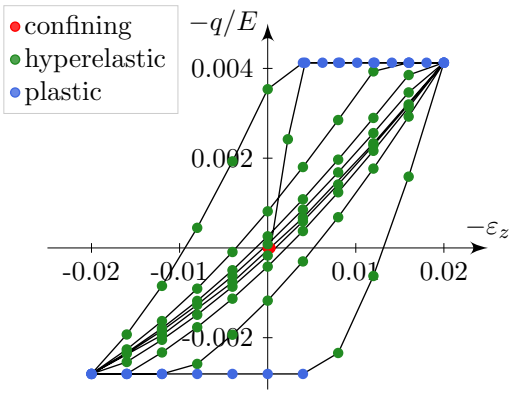

(a) Deviatoric stress $q = \sigma_x - \sigma_z$ vs. axial strain ε_z.

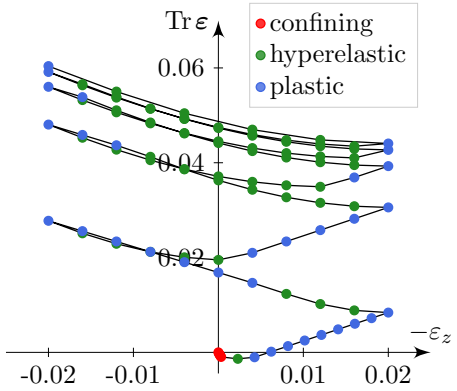

(b) Volumetric strain $\operatorname{Tr}\boldsymbol{\varepsilon}$ vs. axial strain ε_z.

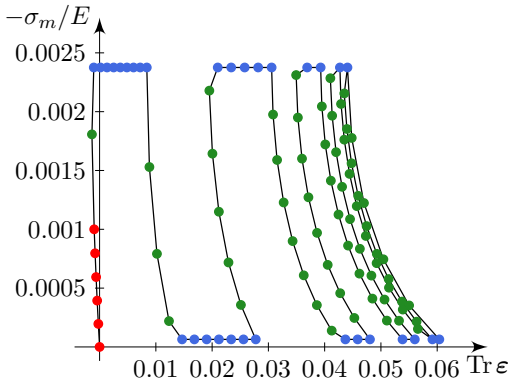

(c) Average stress σ_m vs. volumetric strain $\operatorname{Tr}\boldsymbol{\varepsilon}$.

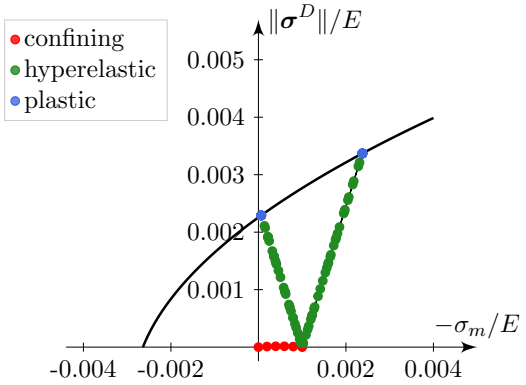

(d) Evolution in the stress domain.

Figure 4: Graphs of cyclic test. The different stages of the evolution are shown with different colors: hydrostatic confining (*red*), hyperelastic (*green*), and plastic (*blue*) stage.

4.3 Cyclic triaxial test

Now, we consider a cyclic triaxial test. As in the previous subsection, we perform initially a hydrostatic compression; then, we decrease and increase cyclically the axial strain ε_z maintaining the lateral pressure constant. The parameters are again fixed by (4.4), and the results are displayed in Figure 4. Notice that the main influence of hyperelasticity, besides the nonlinear evolution of $\operatorname{Tr}\boldsymbol{\varepsilon}$, σ_m, and q, is the progressive accommodation of the values. This is particularly relevant for the saturation of dilatancy, Figure 4b. Furthermore, Figure 4d shows the piecewise linear evolution in the stress space:

$$\|\boldsymbol{\sigma}^D\| = \sqrt{6}\,|\sigma_m + p_0|, \tag{4.10}$$

by (4.3). The intersections of the parabolic domain with (4.10) represent the values of the stress during the plastic phases: $\boldsymbol{P}_1$ (4.6) when $\dot{\varepsilon}_z < 0$ and

$$\begin{aligned}\boldsymbol{P}_2 &\coloneqq (\sigma_{2,m}, \|\boldsymbol{\sigma}_2^D\|)\\ &= \left(\frac{-2(\beta_m + 6a^2\beta^D)p_0 - a + 2\beta_m b - a^2 + \sqrt{\Delta_2}}{2(\beta_m + 6a^2\beta^D)}, -\sqrt{6}\,\frac{-a + 2\beta_m b - a^2 + \sqrt{\Delta_2}}{2(\beta_m + 6a^2\beta^D)}\right),\end{aligned} \tag{4.11}$$

where

$$\Delta_2 \coloneqq a^2(1 + a^2) + 4(\beta_m + 6a^2\beta^D)a^2 p_0 - 4\beta_m a^2 b + 24\beta^D a^2 b(a - \beta_m b),$$

when $\dot{\varepsilon}_z > 0$.

The dilatancy saturation shown in Figure 4b, as well as the accommodation of volumetric strain shown in Figure 4c, are two sides of the same process: the loading path presented in the generalized forces space is progressively drifting towards higher compression values. This process is due to the total strain increase and the presence of hyperelastic coupling, so even if we start the first loading loop with an amplitude sufficient to reach the plastification boundary, the cycling will shift the loading to a purely hyperelastic phase, see Figures 4a, 4b and 4c. This result is a very distinguished feature of the hyperelastic description we have introduced.

4.4 Comparison with an elastic model with linear failure criterion

As it was mentioned in the previous subsection, we have obtained some non-trivial results for the cyclic loading test with the current hyperelastic model: the process of accommodation of volumetric strain and the saturation of dilatancy. That is why we found it important to make a focus in this subsection on the comparison of the responses obtained with the hyperelastic model with parameters (4.4), and with an elastic model (2.2) with linear plasticity criterion for the tests of subsections 4.2 and 4.3. In particular, for the latter model, we consider the linear yield criterion passing through $\boldsymbol{P}_1$ (4.6) and $\boldsymbol{P}_2$ (4.11).

Figure 5 and 6 display the results of monotonic and cyclic triaxial tests with a confining pressure, respectively. The colors identifying the different stages of the evolutions (confining, hyperelastic/elastic, and plastic) are the same as the previous subsections (*red*, *green*, and *blue*). In addition, empty circles represent the response of the hyperelastic model, while diamonds of the elastic model.

For both models and loadings, the evolution of the stress in the reversibility domain lies on the piecewise straight-line defined by (4.10), see Figure 5d and 6d. From Figure 5b and 5c, it is evident that the elastic model provides a linear evolution while the hyperelastic model a nonlinear one. Furthermore, the slope of dilatancy evolution is smaller with the hyperelastic model, as shown by Figure 5b. Finally, Figure 6b and 6c show that only with the hyperelastic model we can achieve the accommodation of the volumetric strain.

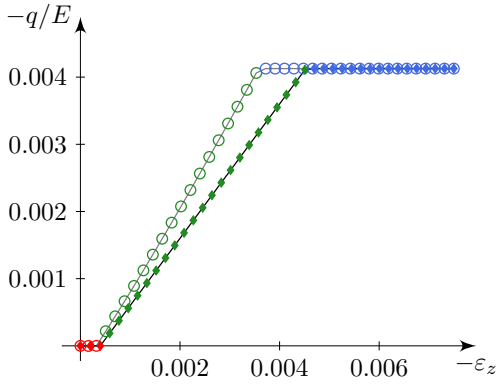

(a) Deviatoric stress $q = \sigma_x - \sigma_z$ vs. axial strain ε_z.

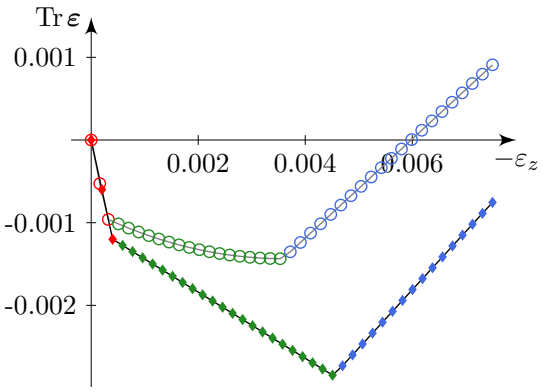

(b) Volumetric strain $\mathrm{Tr}\,\boldsymbol{\varepsilon}$ vs. axial strain ε_z.

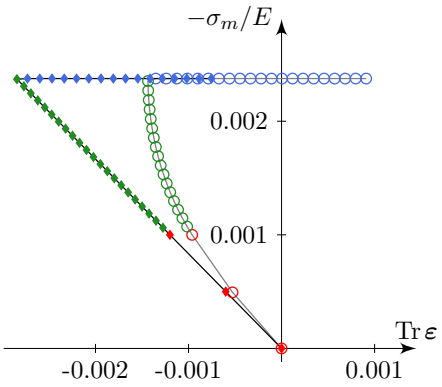

(c) Average stress σ_m vs. volumetric strain $\mathrm{Tr}\,\boldsymbol{\varepsilon}$.

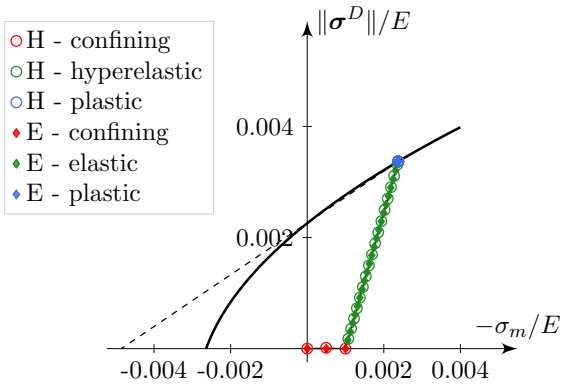

(d) Evolution in the stress domain.

Figure 5: Comparison of the response for a triaxial compression test with a confining pressure. The different stages of the evolution are shown with different colors: hydrostatic confining (*red*), hyperelastic (*green*), and plastic (*blue*) stage. The hyperelastic response is represented with empty circles, while the elastic one with diamonds.

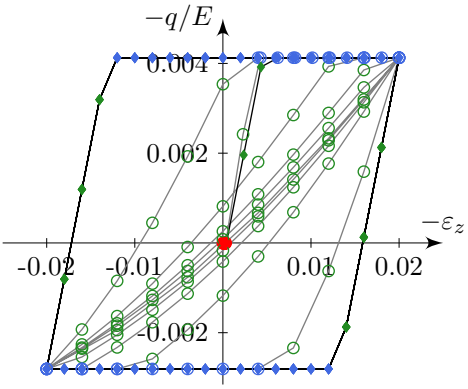

(a) Deviatoric stress $q = \sigma_x - \sigma_z$ vs. axial strain ε_z.

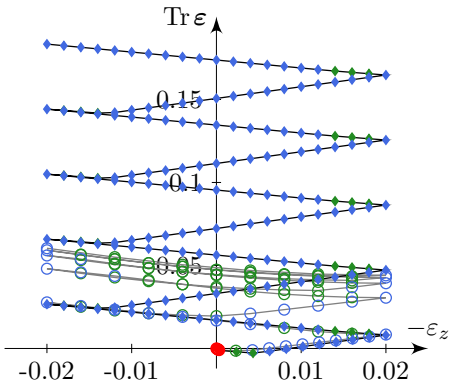

(b) Volumetric strain $\operatorname{Tr}\boldsymbol{\varepsilon}$ vs. axial strain ε_z.

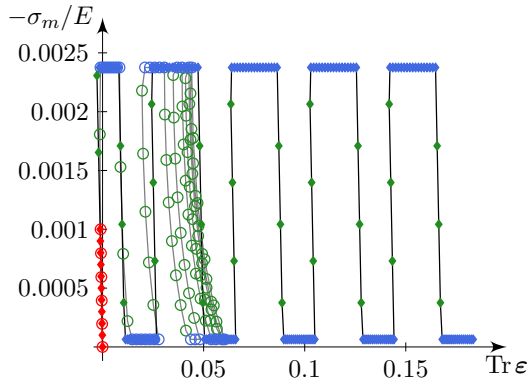

(c) Average stress σ_m vs. volumetric strain $\operatorname{Tr}\boldsymbol{\varepsilon}$.

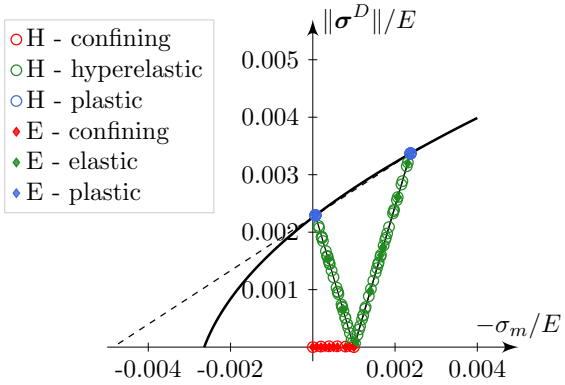

(d) Evolution in the stress domain.

Figure 6: Comparison of the response for a cyclic test. The different stages of the evolution are shown with different colors: hydrostatic confining (*red*), hyperelastic (*green*), and plastic (*blue*) stage. The hyperelastic response is represented with empty circles, while the elastic one with diamonds.

4.5 Radial loadings

In this last numerical example, we consider some radial tests with fixed stress triaxiality, i.e., loadings in which the ratio $\eta := \dfrac{q}{\sigma_m}$ is constant during a compression. Assuming that

$$\boldsymbol{\sigma} = \begin{pmatrix} \sigma_x & 0 & 0 \\ 0 & \sigma_x & 0 \\ 0 & 0 & \sigma_z \end{pmatrix} \qquad \text{and} \qquad \boldsymbol{\varepsilon} = \begin{pmatrix} \varepsilon_x & 0 & 0 \\ 0 & \varepsilon_x & 0 \\ 0 & 0 & \varepsilon_z \end{pmatrix},$$

we have

$$\eta = 3\frac{\sigma_z - \sigma_x}{2\sigma_x + \sigma_z} = \pm\sqrt{\frac{3}{2}}\frac{\|\boldsymbol{\sigma}^D\|}{\sigma_m} = const,$$

which corresponds to

$$\sigma_z = \frac{3 + 2\eta}{3 - \eta}\sigma_x, \qquad \eta \in \mathbb{R}.$$

Figure 7 shows the elastic radial evolution for five different values for η and the parameters (4.4). The case $\eta = 0$ (*violet*) corresponds to a hydrostatic compression, i.e., $\|\boldsymbol{\sigma}^D\| = \mathbf{0}$

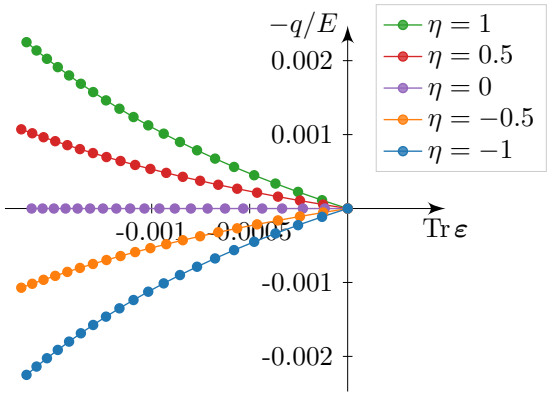

(a) Deviatoric stress q vs. volumetric strain $\mathrm{Tr}\,\boldsymbol{\varepsilon}$.

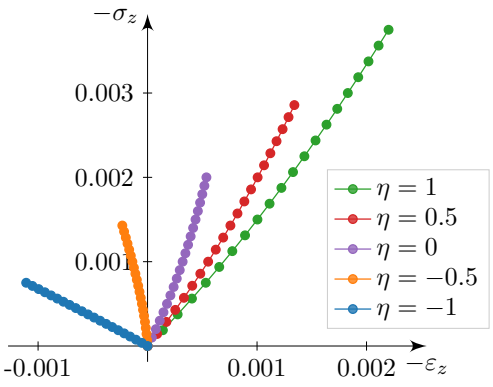

(b) Axial stress σ_z vs. axial strain ε_z.

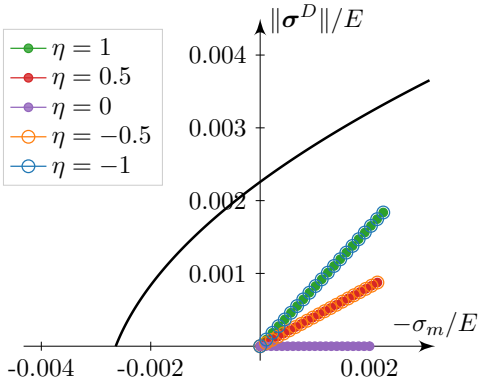

(c) Evolution in the stress domain.

Figure 7: Graphs of radial loadings with different values of $\eta = q/\sigma_m$.

and $\boldsymbol{\sigma}$ lies on the hydrostatic axis in Figure 7c. For all the other cases, one can notice a nonlinear behavior in the $(q, \mathrm{Tr}\,\boldsymbol{\varepsilon})$–space, Figure 7a. This kind of behavior can be observed for some geomaterial, we cite for example [28, Figure 9]. In the stress space, the evolution is linear, Figure 7c, and the angle θ with the hydrostatic axis depends on the absolute value of η:

$$\tan\theta = -\sqrt{\frac{2}{3}}|\eta|.$$

To conclude, while during the radial loading the evolution is still linear in stress space, the stress-strain relation exhibits a clear nonlinear signature.

5 Conclusions

In this paper, we have studied the influence of hyperelasticity on the classical perfect plasticity constitutive behavior. Inspired by the early works of Houlsby and co-authors [21, 4] on specific forms of Gibbs free energy, we explore restrictions imposed on a simplified Helmholtz free energy expression through elastic domain observation. We establish first the nonlinear transformation of the formally defined thermodynamic forces to the experimentally observable mechanical stresses. Our general observation is that the non-linearity coupling influences the thermodynamic-to-experimental mapping of the reversibility region. It is shown then that, for a particular class of hyperbolic elasticity, the hyperelastic

coupling creates a link between a linear criterion in the generalized force space and a quadratic one in the stress space. On one hand, the Hoek–Brown criterion, empirically found long ago, appears to be the natural choice for geomaterials that exhibit nonlinear elastic behavior. On the other hand, in the case of elastic nonlinearity, the simple fact of observing a fixed-in-stress-space yield surface (independent of the plastification level) can point out the two-parameter hyperbolic elasticity relation, which is easier to fit with experimental data. Furthermore, we have numerically implemented an example of this hyperelastic-plastic model written in the formalism of Standard Generalized Materials, ensuring dissipation positivity. The model has been constructed from an energy function with hyperbolic elastic dependencies in the compressibility and shear moduli. The mechanical properties of the presented model have been investigated in detail. Most notably, the obtained model reveals accommodation of dilatancy during cyclic triaxial compression tests with a confining pressure. Being common for many geomaterials and experimentally observed, this saturation of dilatancy constitutes another indirect proof of the importance of hyperelasticity. For sure, the simplified example model defined here can hardly represent all aspects of the rather complex behavior of real geomaterials. Nevertheless, it can be considered as a limiting or initial constitutive relation, serving as a fundamental brick for more subtle models. The authors foresee some relevant modifications that hyperelasticity would provide for previously proposed damage coupled to plasticity law [30].

Statements and Declarations

The authors declare that they have no conflict of interest.

This project received funding from the European Union's Horizon 2020 research and innovation program EURAD under EC grant agreement No 847593.

Acknowledgements

The authors would like to acknowledge G. Bacquaert, F. Escoffier, S. Raude (EDF R&D Palaiseau, France), and C. Stolz (IMSIA, CNRS, France) for numerous fruitful discussions. We thank the CIH team of EDF Hydro (Chambéry, France) for their support and technical advice.

A Implementation considerations

In this section, we propose some considerations about the implementation of the constitutive relation determined by (3.6), the plasticity criterion (3.10), and the normal flow rule (3.11).

With the aim of computing the evolution of a material point under the hypothesis of a quasi-static nonlinear problem, we discretize the problem using an incremental approach. For simplicity, for any tensor or scalar variable x, its value at the previous equilibrium state, at the current equilibrium state, and its increment are denoted by x^-, x and $\Delta x := x - x^-$, respectively. Then, in order to solve locally the evolution of a point we have to satisfy the

following equations:

$$\boldsymbol{\sigma} = \mathbb{E}(\operatorname{Tr}\boldsymbol{\varepsilon})(\boldsymbol{\varepsilon}-\boldsymbol{p}) + \frac{1}{2}\frac{\partial \mathbb{E}(\operatorname{Tr}\boldsymbol{\varepsilon})}{\partial \operatorname{Tr}\boldsymbol{\varepsilon}}(\boldsymbol{\varepsilon}-\boldsymbol{p}):(\boldsymbol{\varepsilon}-\boldsymbol{p}), \qquad \text{(definition of } \boldsymbol{\sigma}\text{)} \tag{A.1}$$

$$\boldsymbol{X} = \mathbb{E}(\operatorname{Tr}\boldsymbol{\varepsilon})(\boldsymbol{\varepsilon}-\boldsymbol{p}), \qquad \text{(definition of } \boldsymbol{X}\text{)} \tag{A.2}$$

$$f_{\boldsymbol{X}}(\boldsymbol{X}) \leq 0, \qquad \text{(yield criterion)} \tag{A.3}$$

$$\Delta\boldsymbol{p} = \Delta\lambda\frac{\partial f_{\boldsymbol{X}}(\boldsymbol{X})}{\partial \boldsymbol{X}}, \Delta\lambda \geq 0, \qquad \text{(flow rule)} \tag{A.4}$$

$$f_{\boldsymbol{X}}(\boldsymbol{X})\Delta\lambda = 0. \qquad \text{(plastic evolution)} \tag{A.5}$$

Here, $\boldsymbol{\varepsilon}$, $\boldsymbol{p}^-$, and, as a consequence, $\boldsymbol{\sigma}^-$ and $\boldsymbol{X}^-$ are known, and the goal is to find the current values $\boldsymbol{p}$, $\boldsymbol{\sigma}$, and $\boldsymbol{X}$. The implementation of this system is composed of two main blocks which correspond to the phase of elastic prediction and to the phase of correction with elasto-plastic evolution.

Remark 5 (Stress computation). The stress tensor $\boldsymbol{\sigma}$ can be computed directly from $\boldsymbol{X}$ thanks to the relation (3.8), instead of using the explicit expression (A.1). As a consequence, for simplicity, in the following, we will only consider (A.2)–(A.5), for which the unknowns are $\Delta\boldsymbol{p}$, $\boldsymbol{X}$, and $\Delta\lambda$.

During the phase of elastic prediction, we define

$$\boldsymbol{X}^{\text{pred}} := \mathbb{E}(\operatorname{Tr}\boldsymbol{\varepsilon})(\boldsymbol{\varepsilon}-\boldsymbol{p}^-).$$

If $f_{\boldsymbol{X}}(\boldsymbol{X}^{\text{pred}}) \leq 0$, then the solution is simply

$$(\Delta\boldsymbol{p}, \boldsymbol{X}, \Delta\lambda) = (\boldsymbol{0}, \boldsymbol{X}^{\text{pred}}, 0).$$

Otherwise, we have to find $(\Delta\boldsymbol{p}, \boldsymbol{X}, \Delta\lambda) \in \mathbb{R}^{3\times3}_{\text{sym}} \times \mathbb{R}^{3\times3}_{\text{sym}} \times \mathbb{R}^+$ such that

$$\begin{cases} \boldsymbol{X} = \mathbb{E}(\operatorname{Tr}\boldsymbol{\varepsilon})(\boldsymbol{\varepsilon}-\boldsymbol{p}^- - \Delta\boldsymbol{p}), \\ \Delta\boldsymbol{p} = \Delta\lambda\dfrac{\partial f_{\boldsymbol{X}}(\boldsymbol{X})}{\partial \boldsymbol{X}}, \\ f_{\boldsymbol{X}}(\boldsymbol{X}) = 0. \end{cases} \tag{A.6}$$

Remark 6. The system (A.6) with unknowns $(\Delta\boldsymbol{p}, \boldsymbol{X}, \Delta\lambda) \in \mathbb{R}^{3\times3}_{\text{sym}} \times \mathbb{R}^{3\times3}_{\text{sym}} \times \mathbb{R}^+$ has a symmetric Jacobian:

$$\tilde{\mathbb{J}} = \begin{pmatrix} \mathbb{E}(\operatorname{Tr}\boldsymbol{\varepsilon}) & \mathbf{I}_4 & \boldsymbol{0} \\ \mathbf{I}_4 & -\Delta\lambda\dfrac{\partial^2 f_{\boldsymbol{X}}(\boldsymbol{X})}{\partial \boldsymbol{X}^2} & -\dfrac{\partial f_{\boldsymbol{X}}(\boldsymbol{X})}{\partial \boldsymbol{X}} \\ \boldsymbol{0} & -\dfrac{\partial f_{\boldsymbol{X}}(\boldsymbol{X})}{\partial \boldsymbol{X}} & 0 \end{pmatrix},$$

where $\mathbf{I}_4$ denotes the fourth-order identity tensor. As a consequence, we can easily define an energy function $\tilde{\phi}(\Delta\boldsymbol{p}, \boldsymbol{X}, \Delta\lambda)$ such that solving the problem (A.6) is equivalent to finding an extremum of $\tilde{\phi}$. In particular,

$$\tilde{\phi}(\Delta\boldsymbol{p}, \boldsymbol{X}, \Delta\lambda) = \frac{1}{2}\mathbb{E}(\operatorname{Tr}\boldsymbol{\varepsilon})\Delta\boldsymbol{p}:\Delta\boldsymbol{p} + \Delta\boldsymbol{p}:\big(\boldsymbol{X} - \mathbb{E}(\operatorname{Tr}\boldsymbol{\varepsilon})(\boldsymbol{\varepsilon}+\boldsymbol{p}^-)\big) - \Delta\lambda f_{\boldsymbol{X}}(\boldsymbol{X})$$

By defining the elastic part of the strain tensor as $\boldsymbol{\varepsilon}^{\mathrm{el}} \coloneqq \boldsymbol{\varepsilon} - \boldsymbol{p}$, we have

$$\begin{cases} \boldsymbol{X} = \mathbb{E}(\operatorname{Tr}\boldsymbol{\varepsilon})(\boldsymbol{\varepsilon}^{\mathrm{el},-} + \Delta\boldsymbol{\varepsilon}^{\mathrm{el}}), & \text{(A.7a)} \\ \Delta\boldsymbol{\varepsilon}^{\mathrm{el}} = \Delta\boldsymbol{\varepsilon} - \Delta\boldsymbol{p}, & \text{(A.7b)} \\ \Delta\boldsymbol{p} = \Delta\lambda \left(\dfrac{1}{\sqrt{6}} \dfrac{\boldsymbol{\varepsilon}^{\mathrm{el,D},-} + \Delta\boldsymbol{\varepsilon}^{\mathrm{el,D}}}{\|\boldsymbol{\varepsilon}^{\mathrm{el,D},-} + \Delta\boldsymbol{\varepsilon}^{\mathrm{el,D}}\|} + \dfrac{a}{3}\mathbf{I}_2 \right), & \text{(A.7c)} \\ \dfrac{2}{\sqrt{6}}\mu(\operatorname{Tr}\boldsymbol{\varepsilon})\|\boldsymbol{\varepsilon}^{\mathrm{el,D},-} + \Delta\boldsymbol{\varepsilon}^{\mathrm{el,D}}\| + aK(\operatorname{Tr}\boldsymbol{\varepsilon})\operatorname{Tr}(\boldsymbol{\varepsilon}^{\mathrm{el},-} + \Delta\boldsymbol{\varepsilon}^{\mathrm{el}}) - b = 0. & \text{(A.7d)} \end{cases}$$

Notice that the last two equations do not depend explicitly on $\boldsymbol{X}$ anymore, and the latter can be easily computed once we have the increment $\Delta\boldsymbol{\varepsilon}^{\mathrm{el}}$. As a consequence, substituting (A.7c) into (A.7b) the problem is reduced to: Find $(\Delta\boldsymbol{\varepsilon}^{\mathrm{el}}, \Delta\lambda) \in \mathbb{R}^{3\times3}_{\mathrm{sym}} \times \mathbb{R}^{+}$ such that

$$\begin{cases} \Delta\boldsymbol{\varepsilon}^{\mathrm{el}} - \Delta\boldsymbol{\varepsilon} + \Delta\lambda \left(\dfrac{1}{\sqrt{6}} \dfrac{\boldsymbol{\varepsilon}^{\mathrm{el,D},-} + \Delta\boldsymbol{\varepsilon}^{\mathrm{el,D}}}{\|\boldsymbol{\varepsilon}^{\mathrm{el,D},-} + \Delta\boldsymbol{\varepsilon}^{\mathrm{el,D}}\|} + \dfrac{a}{3}\mathbf{I}_2 \right) = \mathbf{0}, \\ \dfrac{2}{\sqrt{6}}\mu(\operatorname{Tr}\boldsymbol{\varepsilon})\|\boldsymbol{\varepsilon}^{\mathrm{el,D},-} + \Delta\boldsymbol{\varepsilon}^{\mathrm{el,D}}\| + aK(\operatorname{Tr}\boldsymbol{\varepsilon})\operatorname{Tr}(\boldsymbol{\varepsilon}^{\mathrm{el},-} + \Delta\boldsymbol{\varepsilon}^{\mathrm{el}}) - b = 0. \end{cases}$$

This nonlinear problem can be solved with some iterative methods like the Newton method, for which we have to compute the Jacobian matrix:

$$\mathbb{J} = \begin{pmatrix} \mathbb{J}_1 & \mathbb{J}_2 \\ \mathbb{J}_3 & 0 \end{pmatrix},$$

where

$$\mathbb{J}_1 \coloneqq \mathbf{I}_4 + \frac{\Delta\lambda}{\sqrt{6}} \left[\left(\mathbf{I}_4 - \frac{1}{3}\mathbf{I}_2 \otimes \mathbf{I}_2 \right) \frac{1}{\|\boldsymbol{\varepsilon}^{\mathrm{el,D},-} + \Delta\boldsymbol{\varepsilon}^{\mathrm{el,D}}\|} - \frac{(\boldsymbol{\varepsilon}^{\mathrm{el,D},-} + \Delta\boldsymbol{\varepsilon}^{\mathrm{el,D}}) \otimes (\boldsymbol{\varepsilon}^{\mathrm{el,D},-} + \Delta\boldsymbol{\varepsilon}^{\mathrm{el,D}})}{\|\boldsymbol{\varepsilon}^{\mathrm{el,D},-} + \Delta\boldsymbol{\varepsilon}^{\mathrm{el,D}}\|^3} \right],$$

$$\mathbb{J}_2 \coloneqq \frac{1}{\sqrt{6}} \frac{\boldsymbol{\varepsilon}^{\mathrm{el,D},-} + \Delta\boldsymbol{\varepsilon}^{\mathrm{el,D}}}{\|\boldsymbol{\varepsilon}^{\mathrm{el,D},-} + \Delta\boldsymbol{\varepsilon}^{\mathrm{el,D}}\|} + \frac{a}{3}\mathbf{I}_2,$$

$$\mathbb{J}_3 \coloneqq \frac{2}{\sqrt{6}}\mu(\operatorname{Tr}\boldsymbol{\varepsilon}) \frac{\boldsymbol{\varepsilon}^{\mathrm{el,D},-} + \Delta\boldsymbol{\varepsilon}^{\mathrm{el,D}}}{\|\boldsymbol{\varepsilon}^{\mathrm{el,D},-} + \Delta\boldsymbol{\varepsilon}^{\mathrm{el,D}}\|} + aK(\operatorname{Tr}\boldsymbol{\varepsilon})\mathbf{I}_2,$$

and $\otimes$ denotes the tensor product.

B Hyperelasticity of small rotations

In this section, we will briefly describe finite strain transformation under the assumption of small rotations. The main aim is to justify the choice of infinitesimal strain as the primary state variable and discuss its relevance even for cases going beyond linear approximation. More details may be found in the classical book [40], and some useful numerical examples are also available online https://www.continuummechanics.org/.

Let us suppose that the mechanical system evolves so that any initial vector $\mathbf{X}$ pointing somewhere inside the material transforms to the final position $\mathbf{x}$. Adopting the Lagrange description, we may formally write that $\mathbf{x}$ is some function of $\mathbf{X}$: $\mathbf{x} = \chi(\mathbf{X})$. The first approximation to the deformation generated by the transformation χ in the vicinity of the point $\mathbf{X}$ is given by the function gradient tensor field $\mathbf{F} = \nabla\chi(\mathbf{X})$. If the knowledge of this first approximation suffices to determine the stress at any $\mathbf{X}$, the corresponding material

is called *simple* [40]. For these simple materials the Cauchy stress tensor, which defines the state of local forces, is supposed to be a function of displacement gradient $\mathbf{F}$:

$$\boldsymbol{\sigma} = \boldsymbol{\sigma}(\mathbf{F}). \tag{B.1}$$

For composed transformations $\mathbf{X} \Rightarrow \mathbf{x}_1 \Rightarrow \mathbf{x}_2$ the superposition rule applies. That allows us to discretize any evolution into a sequence of step-by-step transformations:

$$\mathbf{x}_2 = \chi_{21}(\mathbf{x}_1) \text{ and } \mathbf{x}_1 = \chi_{10}(\mathbf{X}),\ \mathbf{F}_{20} = \mathbf{F}_{21} \cdot \mathbf{F}_{10}$$

The attentive reader may remark that the expression (B.1) is not fully consistent, provided the fact that rigid body rotation should not generate any internal forces: $\boldsymbol{\sigma} = 0$ for $\mathbf{F} = \mathbf{F}^{-\dagger} \neq \mathbf{I}_2$. We need then to introduce some supplementary ingredients into this dependence so it becomes fully coherent.

We remind you that any tensor can be decomposed in two different ways that will be useful for our future analysis: polar and symmetric decomposition. The polar decomposition presents the initial tensor as the product of rotation $\mathbf{R}$ and stretching $\mathbf{U}$: $\mathbf{F} = \mathbf{RU}$, where $\mathbf{R}^\dagger\mathbf{R} = \mathbf{I}_2$ and $\mathbf{U} = \mathbf{U}^\dagger$. Alternatively, we can decompose the initial tensor into a sum of symmetric and antisymmetric contributions: $\mathbf{F} = \mathbf{F}_s + \mathbf{F}_a$, where $\mathbf{F}_s^\dagger = \mathbf{F}_s$ and $\mathbf{F}_a^\dagger = -\mathbf{F}_a$. As both decompositions are constructed from the initial tensor $\mathbf{F}$, it can be seen as some bijective function relying on both representations couple: $(\mathbf{F}_s, \mathbf{F}_a) \Leftrightarrow (\mathbf{R}, \mathbf{U})$. We can formally write that:

$$\begin{cases} \mathbf{F}_s = \dfrac{1}{2}(\mathbf{F} + \mathbf{F}^\dagger) = \dfrac{1}{2}(\mathbf{RU} + \mathbf{UR}^\dagger) \\ \mathbf{F}_a = \dfrac{1}{2}(\mathbf{F} - \mathbf{F}^\dagger) = \dfrac{1}{2}(\mathbf{RU} - \mathbf{UR}^\dagger), \end{cases} \tag{B.2}$$

$$\begin{cases} \mathbf{U} = \sqrt{(\mathbf{F}_s - \mathbf{F}_a) \cdot (\mathbf{F}_s + \mathbf{F}_a)} \\ \mathbf{R} = (\mathbf{F}_s + \mathbf{F}_a) \cdot ((\mathbf{F}_s - \mathbf{F}_a)(\mathbf{F}_s + \mathbf{F}_a))^{-1/2}. \end{cases} \tag{B.3}$$

While the first relation (B.2) is trivial, the second one (B.3) is not easy to derive as it relies on advanced tensor analysis methods. Let us notice at this stage that $\mathbf{F}_s$ is directly related to the classical infinitesimal strain $\boldsymbol{\varepsilon}$: $\mathbf{F}_s \equiv \boldsymbol{\varepsilon} + \mathbf{I}_2$. As the latter is supposed to be an objective measure of deformations in this approximation, one may expect that symmetric decomposition is somehow more suitable for small transformations. It's clear, that comprehension of the physical meaning of both decompositions lies at the core of their relevant usage.

We will now address a more general case of finite transformations and understand the mechanical meaning of polar decomposition. If we apply the principle of material frame indifference (MFI) that asserts invariance under superposed rigid motion, it can be shown that the deformation measure cannot be dependent on the rotational part of the decomposition [40]. In other words, stress should be an exclusive function of $\mathbf{U}$, which is said to be objective observable for deformations. For locally invertible transformations, $\det(\mathbf{F}) \neq 0$, the polar decomposition is unique and $\mathbf{U} = \sqrt{\mathbf{F}^\dagger\mathbf{F}}$. Provided the fact that computation of a square root of a positively defined tensor is a rather challenging task, the material constitutive relation is usually written straight with the help of the so-called "Right Cauchy-Green Deformation Tensor" replacing the previous formal expression (B.1) by:

$$\boldsymbol{\sigma} = \boldsymbol{\sigma}(\mathbf{F}) \Rightarrow \ \mathbf{MFI} \ \Rightarrow \boldsymbol{\sigma} = \boldsymbol{\sigma}(\mathbf{U}) \sim \boldsymbol{\sigma}(\mathbf{U}^2) = \boldsymbol{\sigma}(\mathbf{F}^\dagger\mathbf{F}). \tag{B.4}$$

We remark that for small deformations the Cauchy–Green tensor is close to the identity, i.e., $\mathbf{F}^\dagger\mathbf{F} \approx \mathbf{I}_2$, and this is why it is sometimes more convenient to introduce its shifted to zero equivalent, called in the literature the Green–Lagrange strain: $\mathbf{E} \equiv (\mathbf{F}^\dagger\mathbf{F} - \mathbf{I}_2)/2$.

If we summarize, the constitutive relation for simple materials is a relation between Cauchy stress and one of the multiple versions of the objective strain measures (stretching, Cauchy-Green Deformation, Green-Lagrange strain), while the transformation gradient itself (i.e., $\boldsymbol{F}$) is used in the construction of incremental evolution, but being not objective, it's not an appropriate measure for deformations in stress dependence expression.

B.1 Infinitesimal strain

Let us now establish a connection between finite and infinitesimal transformations. For small deformations, the Cauchy stress is supposed to be a function of the infinitesimal strain. It relies on the notion of the displacement field, which is defined for any material point as the vector field $\boldsymbol{u} = \mathbf{x} - \mathbf{X}$. Its gradient is related to the transformation gradient introduced earlier by $\mathbf{F} = \nabla\boldsymbol{u} + \mathbf{I}_2$. Finally, the infinitesimal strain is given by:

$$\boldsymbol{\varepsilon} = \frac{1}{2}(\nabla\boldsymbol{u} + (\nabla\boldsymbol{u})^\dagger) = \mathbf{F}_s - \mathbf{I}_2.$$

The most common way to link both descriptions is to decompose up to first order in the displacement gradient the Green–Lagrange strain $\mathbf{E}$:

$$\mathbf{E} = \frac{1}{2}(\mathbf{F}^\dagger\mathbf{F} - \mathbf{I}_2) = \frac{1}{2}([(\nabla\boldsymbol{u})^\dagger + \mathbf{I}_2] \cdot [\nabla\boldsymbol{u} + \mathbf{I}_2] - \mathbf{I}_2) = \boldsymbol{\varepsilon} + \frac{1}{2}(\nabla\boldsymbol{u})^\dagger(\nabla\boldsymbol{u}),$$
$$\mathbf{E} = \frac{1}{2}(\mathbf{F}^\dagger\mathbf{F} - \mathbf{I}_2) = \boldsymbol{\varepsilon} + o(\nabla\boldsymbol{u}).$$

In the first order of displacement gradient, the Green-Lagrange strain is equivalent to the infinitesimal strain. While the antisymmetric part of the transformation gradient $\mathbf{F}_a$ is neglected inside the constitutive relation, its meaning could be restored by more detailed considerations. Let us establish the link between polar and symmetric decomposition for small deformations:

$$\mathbf{U}^2 = \mathbf{U}^\dagger \cdot \mathbf{U} = \mathbf{F}^\dagger\mathbf{R} \cdot \mathbf{R}^\dagger\mathbf{F} = \mathbf{F}^\dagger\mathbf{F} = \mathbf{I}_2 + 2\boldsymbol{\varepsilon} + o(\nabla\boldsymbol{u}).$$

As the Cauchy–Green tensor is symmetric and both of its additive components ($\mathbf{I}_2$ and $2\boldsymbol{\varepsilon}$) commute, the square root is easily computable:

$$\mathbf{U} = \mathbf{I}_2 + \boldsymbol{\varepsilon} + o(\nabla\boldsymbol{u}) = \mathbf{I}_2 + \frac{1}{2}(\nabla\boldsymbol{u} + (\nabla\boldsymbol{u})^\dagger) + o(\nabla\boldsymbol{u}).$$

For small deformations, this tensor is positively defined and can be inverted in order to obtain rotation component $\mathbf{R}$ of polar decomposition:

$$\begin{aligned}\mathbf{R} = \mathbf{F}\mathbf{U}^{-1} &= (\mathbf{I}_2 + \nabla\boldsymbol{u})\left(\mathbf{I}_2 - (\nabla\boldsymbol{u} + \frac{1}{2}(\nabla\boldsymbol{u})^\dagger)\right) + o(\nabla\boldsymbol{u}) \\ &= \mathbf{I}_2 + \frac{1}{2}(\nabla\boldsymbol{u} - (\nabla\boldsymbol{u})^\dagger) + o(\nabla\boldsymbol{u}) \\ &= \mathbf{I}_2 + \mathbf{F}_a + o(\nabla\boldsymbol{u}).\end{aligned}$$

So far, we have obtained a bijective relation between symmetric and polar tensor decomposition $(\mathbf{F}_s, \mathbf{F}_a) \Leftrightarrow (\mathbf{R}, \mathbf{U})$ for the infinitesimal approximation case. The antisymmetric part

of the transformation gradient $\mathbf{F}_a$ represents infinitesimal rotations which are neglected in the stress-strain dependence (B.4), but are present in the full expression of transformation gradient:

$$\mathbf{F} = \mathbf{R}\mathbf{U} = \mathbf{F}_s + \mathbf{F}_a = (\mathbf{I}_2 + \mathbf{F}_a) \cdot (\mathbf{I}_2 + \boldsymbol{\varepsilon}) + o(\nabla \boldsymbol{u}).$$

For composed infinitesimal transformations $\mathbf{X} \Rightarrow \mathbf{x}_1 \Rightarrow \mathbf{x}_2$, the superposition rule simplifies to a separate addition of infinitesimal rotations and infinitesimal strains:

$$\mathbf{x}_2 = \chi_{21}(\mathbf{x}_1) \text{ and } \mathbf{x}_1 = \chi_{10}(\mathbf{X}),\ \boldsymbol{\varepsilon}_{20} = \boldsymbol{\varepsilon}_{21} + \boldsymbol{\varepsilon}_{10} \text{ and } \mathbf{F}_{a,20} = \mathbf{F}_{a,21} + \mathbf{F}_{a,10}.$$

This allows us to discretize once again any evolution into a sequence of step-by-step transformations.

Finally, the classical Hooke's law is obtained by developing Rivlin–Ericksen decomposition up two first-order in displacement gradients:

$$\boldsymbol{\sigma} = c_0\mathbf{I}_2 + c_1\mathbf{E} + c_2\mathbf{E}^2 = \lambda \mathrm{Tr}\,\boldsymbol{\varepsilon}\,\mathbf{I}_2 + 2\mu\boldsymbol{\varepsilon} + o(\nabla \boldsymbol{u}). \tag{B.5}$$

where c_i are some functions of rotational invariants of Green–Lagrange tensor $\mathbf{E}$, and λ and μ are elastic constants (Lamé parameters).

The same equation (B.5) can be derived from the energy-based formulation. First, we introduce Helmholtz free energy, that is a function of rotational invariants of infinitesimal strain $\boldsymbol{\varepsilon}$, which we can formally write as $\phi(\boldsymbol{\varepsilon})$. Second, the Cauchy stress tensor is obtained as dual conjugate to the total strain, i.e., $\boldsymbol{\sigma} = \partial\phi/\partial\boldsymbol{\varepsilon}$. If we want to keep just linear terms in the stress expression, we must use the second-order expansion inside the free energy. Therefore, the free energy related to Hooke's law can depend only on first ($\mathrm{Tr}\,(\boldsymbol{\varepsilon})$) and second ($\mathrm{Tr}\,(\boldsymbol{\varepsilon}^2) \equiv \boldsymbol{\varepsilon} : \boldsymbol{\varepsilon}$) invariants of rotation, as the third one would give higher order terms:

$$\phi(\boldsymbol{\varepsilon}) = \frac{1}{2}\lambda(\mathrm{Tr}\,\boldsymbol{\varepsilon})^2 + \mu\boldsymbol{\varepsilon} : \boldsymbol{\varepsilon} + o((\nabla \boldsymbol{u})^2).$$

In conclusion, Rivlin–Ericksen and Helmholtz's descriptions coincide for infinitesimal strain approximation.

B.2 Small rotations

The goal of this last subsection is to see whether it is possible to extend this most trivial constitutive equation relying on infinitesimal strain deformation's measure for other kinds of approximations. In particular, here we will consider the case of small rotations. By analogy with the previous considerations, we still start from $\mathbf{F} = \mathbf{R}\mathbf{U}$ and we additionally suppose that $\mathbf{R} = \mathbf{I}_2 + \boldsymbol{\Omega}$, where $\boldsymbol{\Omega}$ is small. This leads to:

$$\begin{aligned} \mathbf{R}^\dagger \cdot \mathbf{R} = \mathbf{I}_2 \quad &\Rightarrow \quad \boldsymbol{\Omega} + \boldsymbol{\Omega}^\dagger + \boldsymbol{\Omega}^\dagger \cdot \boldsymbol{\Omega} = 0 \\ \mathbf{R} \cdot \mathbf{R}^\dagger = \mathbf{I}_2 \quad &\Rightarrow \quad \boldsymbol{\Omega} + \boldsymbol{\Omega}^\dagger + \boldsymbol{\Omega} \cdot \boldsymbol{\Omega}^\dagger = 0. \end{aligned}$$

The small rotations are represented once again by the antisymmetric tensor: $\boldsymbol{\Omega} = -\boldsymbol{\Omega}^\dagger + O(\boldsymbol{\Omega}\boldsymbol{\Omega}^\dagger)$. As we have mentioned before, (B.2) polar to symmetric relation is straightforward, so we get:

$$\begin{cases} \mathbf{F}_s = \dfrac{1}{2}((1+\boldsymbol{\Omega})\mathbf{U} + \mathbf{U}(1+\boldsymbol{\Omega}^\dagger)) = \mathbf{U} + \dfrac{1}{2}(\boldsymbol{\Omega}\mathbf{U} + \mathbf{U}\boldsymbol{\Omega}^\dagger) \\ \mathbf{F}_a = \dfrac{1}{2}((1+\boldsymbol{\Omega})\mathbf{U} - \mathbf{U}(1+\boldsymbol{\Omega}^\dagger)) = \dfrac{1}{2}(\boldsymbol{\Omega}\mathbf{U} - \mathbf{U}\boldsymbol{\Omega}^\dagger). \end{cases}$$

Its inverse can be obtained up to any order in the small rotation expansion:

$$\begin{cases} \mathbf{U} = \mathbf{F}_s - \dfrac{1}{2}(\boldsymbol{\Omega}\mathbf{F}_s + \mathbf{F}_s\boldsymbol{\Omega}^\dagger) + \dfrac{1}{4}(\boldsymbol{\Omega}^2\mathbf{F}_s + 2\boldsymbol{\Omega}\mathbf{F}_s\boldsymbol{\Omega}^\dagger + \mathbf{F}_s(\boldsymbol{\Omega}^\dagger)^2) + o(\boldsymbol{\Omega}^2) \\ \mathbf{F}_a = \dfrac{1}{2}(\boldsymbol{\Omega}\mathbf{F}_s - \mathbf{F}_s\boldsymbol{\Omega}^\dagger) - \dfrac{1}{4}(\boldsymbol{\Omega}^2\mathbf{F}_s - \mathbf{F}_s(\boldsymbol{\Omega}^\dagger)^2) + o(\boldsymbol{\Omega}^2). \end{cases}$$

We can now make the first quite trivial conclusion, that for any finite transformation, the stretching tensor is equal to the symmetric part of the transformation gradient for vanishing rotation. We are going further, reminding that $\mathbf{F}_s$ is nothing else as $\mathbf{I}_2 + \boldsymbol{\varepsilon}$, and developing the equation for stretching $\mathbf{U}$ up to the first order in $\boldsymbol{\Omega}$:

$$\mathbf{U} - \mathbf{I}_2 = \boldsymbol{\varepsilon} + \frac{1}{2}(\boldsymbol{\varepsilon}\boldsymbol{\Omega} - \boldsymbol{\Omega}\boldsymbol{\varepsilon}) + O(\boldsymbol{\Omega}^2), \tag{B.6}$$

$$(\mathbf{U} - \mathbf{I}_2)^2 = \boldsymbol{\varepsilon}^2 + \frac{1}{2}(\boldsymbol{\varepsilon}^2\boldsymbol{\Omega} - \boldsymbol{\Omega}\boldsymbol{\varepsilon}^2) + O(\boldsymbol{\Omega}^2). \tag{B.7}$$

The Cauchy stress can be obtained through the Rivlin–Ericksen decomposition, written for convenience for shifted stretching tensor $\mathbf{U} - \mathbf{I}_2$:

$$\boldsymbol{\sigma} = c_0\mathbf{I}_2 + c_1(\mathbf{U} - \mathbf{I}_2) + c_2(\mathbf{U} - \mathbf{I}_2)^2 = c_0\mathbf{I}_2 + c_1\boldsymbol{\varepsilon} + c_2\boldsymbol{\varepsilon}^2 + O(\boldsymbol{\Omega}). \tag{B.8}$$

Even if we use infinitesimal strain as a deformation measure it does not need to be small, since it should be just seen as shifted symmetric part of the transformation gradient: $\boldsymbol{\varepsilon} = (\nabla\boldsymbol{u} + (\nabla\boldsymbol{u})^\dagger)/2 = \mathbf{F}_s - \mathbf{I}_2$. In this expression, the linear terms in the stretching tensor $\boldsymbol{\Omega}$ will appear as they are initially present in the stretching expansion (B.6), for instance, $\boldsymbol{\sigma} \sim \boldsymbol{\varepsilon}\boldsymbol{\Omega} - \boldsymbol{\Omega}\boldsymbol{\varepsilon}$. We will show further that, if we follow the energy approach, these linear terms will disappear in the final constitutive relation.

We make first an interesting remark: while the tensor expressions (B.6) are equal up to the first order in rotation, all of their invariants (trace, deviator, and determinant) are equal up to the second order in rotation. From (B.6) we get the first two invariants:

$$\operatorname{Tr}(\mathbf{U} - \mathbf{I}_2) = \operatorname{Tr}(\boldsymbol{\varepsilon}) + O(\boldsymbol{\Omega}^2)$$
$$\operatorname{Tr}(\mathbf{U} - \mathbf{I}_2)^2 = \operatorname{Tr}(\boldsymbol{\varepsilon}^2) + O(\boldsymbol{\Omega}^2)$$

For the last invariant we have computed first the cube of shifted stretching:

$$(\mathbf{U} - \mathbf{I}_2)^3 = \boldsymbol{\varepsilon}^3 + (\boldsymbol{\varepsilon}^3\boldsymbol{\Omega} - \boldsymbol{\Omega}\boldsymbol{\varepsilon}^3)/2 + O(\boldsymbol{\Omega}^2)$$
$$\operatorname{Tr}(\mathbf{U} - \mathbf{I}_2)^3 = \operatorname{Tr}(\boldsymbol{\varepsilon}^3) + O(\boldsymbol{\Omega}^2).$$

Finally, as all "mechanical" invariants (trace, deviator, determinant) are functions of three traces obtained just above, they would also be equal between shifted stretching $(\mathbf{U} - \mathbf{I}_2)$ and infinitesimal strain $\boldsymbol{\varepsilon}$. The most general hyperelastic isotropic constitutive relation is obtained as the derivative of Helmholtz free energy, that is a function of the three rotational invariants of infinitesimal strain $\boldsymbol{\varepsilon}$ up to the second order approximation in rotation tensor $\boldsymbol{\Omega}$:

$$\phi = \phi(\operatorname{Tr}(\mathbf{U} - \mathbf{I}_2), \operatorname{Tr}(\mathbf{U} - \mathbf{I}_2)^2, \operatorname{Tr}(\mathbf{U} - \mathbf{I}_2)^3) = \phi(\operatorname{Tr}\boldsymbol{\varepsilon}, \operatorname{Tr}(\boldsymbol{\varepsilon}^2), \operatorname{Tr}(\boldsymbol{\varepsilon}^3)) + O(\boldsymbol{\Omega}^2),$$

so we can formally write

$$\phi(\mathbf{U} - \mathbf{I}_2) = \phi(\boldsymbol{\varepsilon}) + O(\boldsymbol{\Omega}^2)$$

and

$$\boldsymbol{\sigma} = d_1\mathbf{I}_2 + d_2(\mathbf{U}-\mathbf{I}_2) + d_3(\mathbf{U}-\mathbf{I}_2)^2 = r_1\mathbf{I}_2 + r_2\boldsymbol{\varepsilon} + r_3\boldsymbol{\varepsilon}^2 + O(\boldsymbol{\Omega}^2). \tag{B.9}$$

where the functions d_n and r_n are the partial derivatives of the free energy ϕ:

$$d_n = n\frac{\partial\phi(\mathbf{U}-\mathbf{I}_2)}{\partial \mathrm{Tr}\,[(\mathbf{U}-\mathbf{I}_2)^n]} \qquad \text{and} \qquad r_n = n\frac{\partial\phi(\boldsymbol{\varepsilon})}{\partial \mathrm{Tr}\,(\boldsymbol{\varepsilon}^n)} \qquad n\in\{1,2,3\}.$$

The main difference between the Rivlin–Ericksen constitutive relation (B.8) and the hyperelastic Helmholtz one (B.9) is that the latter expansion on small rotation does not have any linear in the $\boldsymbol{\Omega}$ term. The explanation of this major difference is that linear terms (for example $\boldsymbol{\sigma} \sim \boldsymbol{\varepsilon}\boldsymbol{\Omega} - \boldsymbol{\Omega}\boldsymbol{\varepsilon}$) result in a non-symmetric tangent operator $\partial\boldsymbol{\sigma}/\partial\boldsymbol{\varepsilon}$, which points out the absence of gradient-generating energy function, thus violating the Clairaut–Schwarz theorem.

We summarize here our main conclusion: *the hyperelastic Helmholtz's description for small rotation approximation results in the very general constitutive relation* (B.9)*, where the infinitesimal strain can still be used as an objective measure of deformation up to the second order in rotations* $\boldsymbol{\Omega}$*.*

References

[1] L. R. Alejano and A. Bobet. Drucker–Prager criterion. *Rock Mechanics and Rock Engineering*, 45:995–999, 2012.

[2] D. Aubry, J. C. Hujeux, F. Lassoudiere, and Y. Meimon. A double memory model with multiple mechanisms for cyclic soil behavior. In *Proceedings of International Symposium on Numerical Models in Geomechanics*, pages 3–13, 1982.

[3] F. L. L. B. Carneiro. A new method to determine the tensile strength of concrete. In *Proceedings of the 5th meeting of the Brazilian Association for Technical Rules ("Associação Brasileire de Normas Técnicas—ABNT")*, pages 126–129, 09 1943.

[4] I. F. Collins and G. T. Houlsby. Application of thermomechanical principles to the modelling of geotechnical materials. *Proceedings of the Royal Society A: Mathematical, Physical, and Engineering Sciences*, 453(1964):1975–2001, 1997.

[5] C. A. Coulomb. Essai sur une application des règles des maximis et minimis à quelquels problèmes de statique, relatifs à l'architecture. *Academie Royale Des Sciences Paris Mem. Math. Phys.*, 7:343–382, 1776.

[6] Y. F. Dafalias and E. P. Popov. A model of nonlinearly hardening materials for complex loading. *Acta Mechanica*, 21:173–192, 1975.

[7] D. C. Drucker and W. Prager. Soil mechanics and plastic analysis or limit design. *Quarterly of Applied Mathematics*, 10:157–165, 1952.

[8] E. Eberhardt. The Hoek-Brown failure criterion. *Rock Mechanics and Rock Engineering*, 45:981–988, 2012.

[9] I. Einav, G.T. Houlsby, and G.D. Nguyen. Coupled damage and plasticity models derived from energy and dissipation potentials. *International Journal of Solids and Structures*, 44(7):2487–2508, 2007.

[10] C. Fairhurst. On the validity of the 'Brazilian' test for brittle materials. *International Journal of Rock Mechanics and Mining Sciences & Geomechanics Abstracts*, 1(4):535–546, 1964.

[11] R. Fernandes, C. Chavant, and R. Chambon. A simplified second gradient model for dilatant materials : theory and numerical implementation. *International Journal of Solids and Structures*, 45:5289–5307, 2008.

[12] P. Germain, Q. S. Nguyen, and P. Suquet. Continuum thermodynamics. *Journal of Applied Mechanics*, 50(4b):1010–1020, 1983.

[13] A. Griffith. The theory of rupture. In *Proc. Ist. Int. Congr. Appl. Mech.*, pages 54–63, 1924.

[14] B. Halphen and Q. S. Nguyen. Sur les matériaux standard généralisés. *Journal de Mécanique*, 14(1):39–63, 01 1975.

[15] T. Helfer and É. Castelier. Le générateur de code `mfront`: présentation générale et application aux propriétés matériau et aux modèles, 2013.

[16] E. Hoek and E. T. Brown. Empirical strength criterion for rock masses. *Journal of the Geotechnical Engineering Division*, 106:1013–1035, 1980.

[17] E. Hoek and E. T. Brown. *Underground Excavation in Rock*. E & FN Spon, 1982.

[18] E. Hoek and E. T. Brown. The Hoek–Brown failure criterion and GSI – 2018 edition. *Journal of Rock Mechanics and Geotechnical Engineering*, 11:445–463, 2019.

[19] E. Hoek and P. Marinos. A brief history of the development of the Hoek–Brown failure criterion. *Soils and Rocks*, 30(2):85–92, 2007.

[20] G. T. Houlsby and A. M. Puzrin. *Principles of Hyperplasticity: An Approach to Plasticity Theory Based on Thermodynamic Principles*. Springer Verlag London Limited, 2007.

[21] G.T. Houlsby. The use of a variable shear modulus in elastic-plastic models for clays. *Computers and Geotechnics*, 1(1):3–13, 1985.

[22] C. Jailin, A. Carpiuc, K. Kazymyrenko, M. Poncelet, H. Leclerc, F. Hild, and S. Roux. Virtual hybrid test control of sinuous crack. *Journal of the Mechanics and Physics of Solids*, 102:239–256, 2017.

[23] L. Knittel, T. Wichtmann, A. Niemunis, G. Huber, E. Espino, and T. Triantafyllidis. Pure elastic stiffness of sand represented by response envelopes derived from cyclic triaxial tests with local strain measurements. *Acta Geotechnica*, 15:2075–2088, 2020.

[24] J. F. Labuz and A. Zang. Mohr–Coulomb failure criterion. *Rock Mechanics and Rock Engineering*, 45:975–979, 2012.

[25] E. Lanoye, F. Cormery, D. Kondo, and J. F. Shao. An isotropic unilateral damage model coupled with frictional sliding for quasi-brittle materials. *Mechanics Research Communications*, 53:31–35, 2013.

[26] S.-K. Lee, Y.-C. Song, and S.-H. Han. Biaxial behavior of plain concrete of nuclear containment building. *Nuclear Engineering and Design*, 227(2):143–153, 2004.

[27] H. Li, T. Guo, Y. Nan, and B. Han. A simplified three-dimensional extension of Hoek–Brown strenght. *Journal of Rock Mechanics and Geotechnical Engineering*, 13:568–578, 2021.

[28] M. P. Luong. Stress–strain aspects of cohesionless soils under cyclic and transient loading. In *Proceedings of the International Symposium on Soils under Cyclic and Transient Loading*, pages 315–324. A. A. Balkema, 01 1980.

[29] J.-J. Marigo. Constitutive relations in plasticity, damage and fracture mechanics based on a work property. *Nuclear Engineering and Design*, 114(3):249–272, 1989.

[30] J.-J. Marigo and K. Kazymyrenko. A micromechanical inspired model for the coupled to damage elastoplastic behavior of geomaterials under compression. *Mechanics & Industry*, 20(105), 2019.

[31] O. Mohr. Welche umstände bedingen die elastizitätsgrenze und den bruch eines materials? *Zeitschrift des Vereines deutscher Ingenieure*, 44:1524–1530, 1900.

[32] A. Niemunis and M. Cudny. On hyperelasticity for clays. *Computers and Geotechnics*, 23:221–236, 1998.

[33] R. W. Ogden. *Non-linear elastic deformations*. Ellis Horwood series in mathematics and its applications. E. Horwood Halsted Press, 1984.

[34] X. D. Pan and J. Hudson. A simplified three-dimensional Hoek-Brown yield criterion. *Proc Symposium on Rock Mechanics and Power Plants*, pages 95–103, 1988.

[35] S. Priest. Three-dimensional failure criteria based on the Hoek-Brown criterion. *Rock Mechanics and Rock Engineering*, 45:989–993, 2012.

[36] S. Raude, F. Laigle, R. Giot, and R. Fernandes. A unified thermoplastic/viscoplastic costitutive model for geomaterials. *Acta Geotechnica*, 11:849–869, 2016.

[37] M. B. Rubin. Physical reasons for abandoning plastic deformation measures in plasticity and viscoplasticity theory. *Archives of Mechanics*, 53:519–539, 2001.

[38] J. C. Simo and T. J. R. Hughes. *Computational inelasticity*, volume 7 of *Interdisciplinary Applied Mathematics*. Springer International Publishing, 1998.

[39] P. Suquet. *Rupture et plasticité*. École Polytechnique, Palaiseau, France, 2003.

[40] C. Truesdell. *A First Course in Rational Continuum Mechanics.* The John Hopkins University, Baltimore, first edition, 1972.

[41] P. A. Veermer and R. de Borst. Non-associated plasticity for soils, concrete and rock. *HERON*, 29(3):1–64, 1984.

[42] Q. Zhang, H. Zhu, and L. Zhang. Modification of a generalized three-dimensional Hoek–Brown strenght criterion. *Internation Journal of Rock Mechanics and Mining Sciences*, 59:80–96, 2013.

[43] Z. Zhou, W. Ma, S. Zhang, Y. Mu, S. Zhao, and G. Li. Yield surface evolution for columnar ice. *Results in Physics*, 6:851–859, 2016.